THESIS

STUDY OF A HIGH POWER CAPILLARY DISCHARGE

Submitted by

Juan Jose Gonzalez

Electrical & Computer Engineering Department

In partial fulfillment of the requirements

for the Degree of Master of Science

Colorado State University

Fort Collins, Colorado

Fall 1999

COLORADO STATE UNIVERSITY

August 18, 1999

WE HEREBY RECOMMEND THAT THE THESIS PREPARED UNDER OUR SUPERVISION BY JUAN JOSE GONZALEZ ENTITLED STUDY OF A HIGH POWER CAPILLARY DISCHARGE BE ACCEPTED AS FULFILLING IN PART REQUIREMENTS FOR THE DEGREE OF MASTER OF SCIENCE.

Committee on Graduate Work

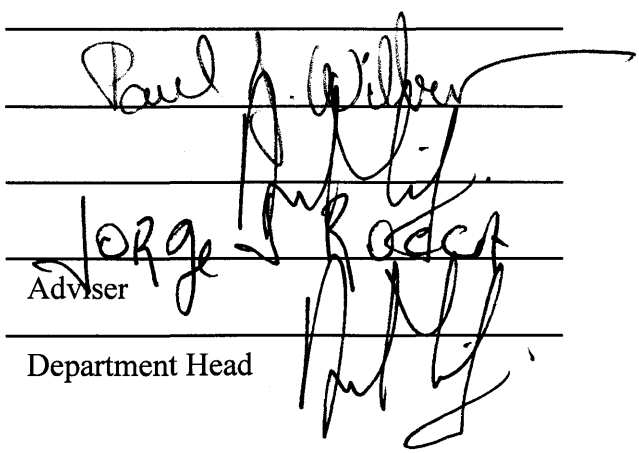

Adviser

Department Head

ABSTRACT OF THESIS

STUDY OF A HIGH POWER CAPILLARY DISCHARGE

The direct generation by electrical discharges of hot and dense plasma columns with large length-to-diameter ratio is of interest for the development of efficient soft x-ray lasers and has resulted in the generation of coherent radiation at wavelength as short as 46.9 nm. This work presents the first experimental results of a new high power density capillary discharge designed to explore the generation of axially uniform plasma columns for the development of discharge pumped lasers at shorter wavelengths. A high power pulsed power generator based on a three-stage pulse compression scheme was developed. The final stage consist of a water dielectric Blumlein transmission line designed to generate current pulses of up to 225 kA with a 10-90 % rise-time of $\cong$ 10 ns through the capillary load. Argon plasmas generated in polyacetal and ceramic capillaries were studied by means of time resolved soft x-ray pinhole camera images and time resolved XUV spectroscopy. The pinhole images show that the current pulse rapidly compresses the plasma to form a column with a soft x-ray emitting region with a diameter of $\approx$ 250 μm. Spectra in the 18-23 nm region are observed to be dominated by an ArXV line.

The experimental data obtain is in agreement with model computations that suggest these discharge conditions should generate plasma columns of $\approx$ 200-300 μm in diameter with electron temperatures > 250 eV and densities of 1-2x10^{20} cm^{-3}.

Juan Jose Gonzalez
Electrical & Computer Engineering Department
Colorado State University
Fort Collins, CO 80523
Fall 1999

TABLE OF CONTENTS

CHAPTER 1

FUNDAMENTALS OF SOFT X-RAY LASERS

1.1. Introduction

Capillary discharge excitation of argon plasma columns has led to the first demonstration of large soft x-ray amplification by collisional excitation in a discharge pumped plasma at 46.9 nm in Ne-like Ar [1.1]. The advantageous characteristic of these capillary plasmas has also allowed for the development of the first saturated table-top soft x-ray amplifier [1.2]. The demonstration of lasing in Ne-like S at 60.8 nm [1.3] has proved the feasibility of producing amplification by capillary discharge excitation in elements that are solid at room temperature, a situation that will be frequently encountered in attempts to extend this scheme to shorter wavelengths. However, the fundamental physics of the generation of amplification by stimulated emission determines a dramatic scaling of the power density deposition required to obtain substantial gain at shorter wavelengths. For example, in the case of a Doppler broadened

laser line, most frequently the dominant line broadening mechanism under soft x-ray laser operating conditions, the power requirement scales as $P \alpha \lambda^{-4}$. In addition, the pump power required for lasing at soft x-ray wavelengths is often further increased by refraction losses that reduce the effective gain coefficient.

Scaling of collisionally excited capillary discharge lasers to wavelength shorter than 46.9 nm, will required the use of elements heavier than argon and higher excitation power densities. The scaling of plasmas conditions and pump requirements for lasing at wavelengths as short as 10 nm have been estimated [1.4]. Figure 1.1 shows the result of this scaling for selected elements in the Ne-like and Ni-like sequences with the estimated plasma parameters necessary to obtain gain in a capillary discharge plasma column [1.4].

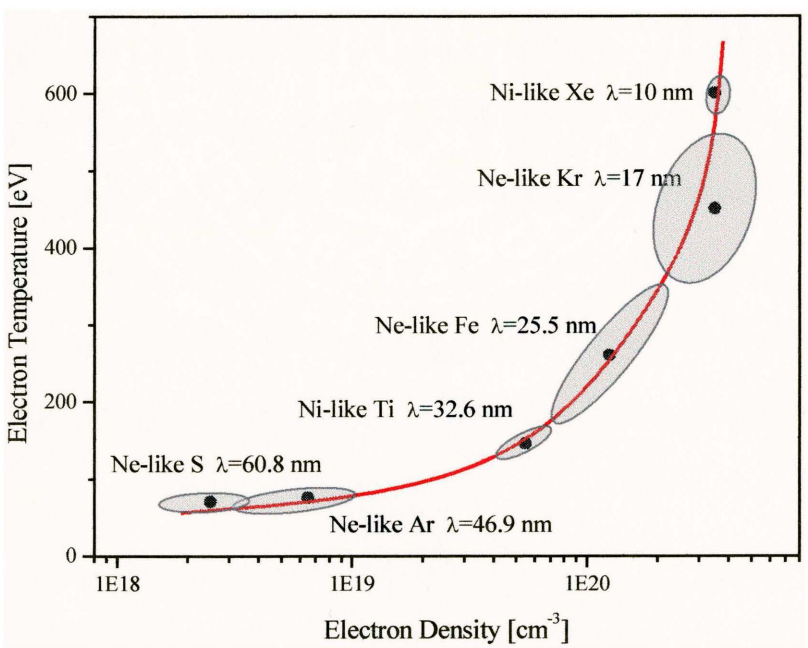

Figure 1.1. Scaling of the soft x-ray laser plasma parameters for selected elements in the Ne-like and Ni-like series.

This dissertation reports results of a study in which capillary discharge plasma columns were generated that are an order of magnitude denser and significantly hotter than those generated by previous capillary discharges [1.5]. The plasma columns here reported were generated by a new high voltage pulse generator that was designed and constructed as part of the work completed during this thesis [1.6]. This new high power density discharge was used to generate argon plasma columns in 3 mm and 4 mm diameter capillaries. To characterize these plasmas time-resolved spectroscopic diagnostics in the soft x-ray spectral region were carried out, and time-resolved images of the plasma column were obtained by means of a x-ray pinhole camera. Different capillary materials were also studied as a way to optimize conditions that maximize the electron temperature.

This introductory chapter discuses the generation of population inversion and gain in the soft x-ray region of the spectrum, which is the main motivation for the development of the discharge described in this thesis. Section 1.2 is a brief introduction to the history soft x-rays lasers and the most important population inversion schemes utilized to produce gain in this spectral region. Section 1.3 describes the generation of plasma columns suitable for x-ray amplification and same of the most successful capillary discharge excitation experiments in which gain have been observed.

1.2. Development of compact soft x-ray lasers

Just three years after the invention of the ruby laser, a paper [1.7] appeared in the Russian literature drawing attention to the potential of recombining plasmas for the generation of gain. Several seminal papers on new schemes for the generation of x-ray

lasing followed based on inner-shell photoionization [1.8], collisionally excitation [1.9,1.10], and photopumping [1.11]. With the announcement in 1984 of the first demonstration of lasing action in the soft x-ray region by groups in Lawrence Livermore National Laboratory [1.12] and Princeton University [1.13] a period of intense work on soft x-ray lasers began.

These two groups used two different population inversion mechanisms to generated gain and these have formed the basis of the successful work on soft x-ray lasers since that time. They are the plasma recombination approach based in on H-like and Li-like ions; and the collisionally excitation approach based on closed shell ions such as Ne-like and Ni-like ions. In the collisional excitation scheme, illustrated in figure 1.2a, the upper level is dominantly populated from the ground state of the same ion by electron collisions. The upper level is chosen such that radiative decay to the ground level is dipole forbidden. The pumping is then followed by lasing through a dipole-allowed transition ($\Delta n = 0$) to a lower state, from which decay occurs very rapidly through radiation to the ground level. The other approach that has resulted in large amplification is the collisional recombination scheme. Collisional (three-body) recombination, in contrast to radiative recombination, populates preferentially highly excited levels. In the collisional recombination approach, free electrons from the continuum are captured into high bound quantum states of the ion. This is followed by collisional cascading down to lower states (see fig. 1.2b). At appropriate electron densities a population inversion can result between the lower quantum state, that is usually rapidly depopulated by radiative decay.

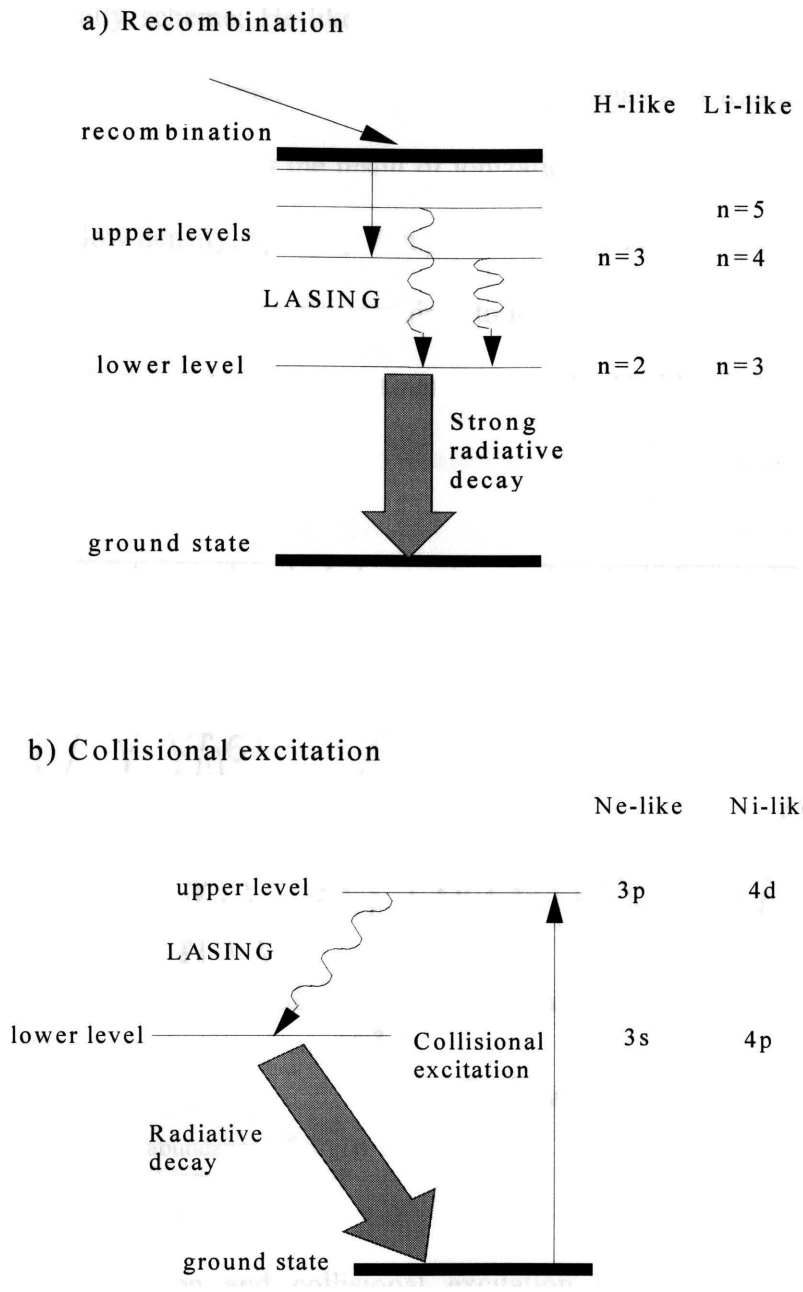

Figure 1.2. Simplified energy level diagram for a) collisional excitation and b) recombination laser schemes.

In the most traditional quasi-steady state implementation of both schemes, the population inversion necessary for stimulated emission and gain is assisted by fast radiative decay of the lower level. Another common feature is that the ion ground state from which the population inversion is supplied has a closed shell (Ne – Ni-like ions for

the collisionally scheme; He-like or bare ions for the recombination scheme). Closed shell ions have a high fractional abundance in plasmas and this aids the generation of high gain. Figure 1.3 shows the result of ionization equilibrium calculations in argon for the case of a low density, optically thin plasma [1.14]. This particular example shows that the jump in the ionization energy, required to ionize configurations with a single electron in the outer shell, results in a high abundance of the Ne-like and He-like species over a wide temperature range.

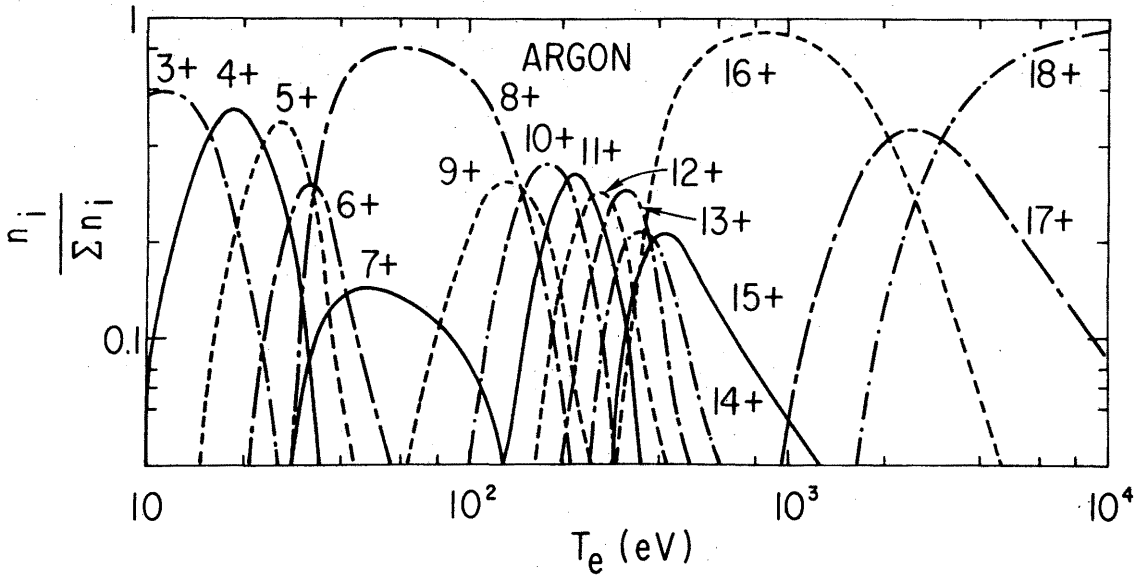

Figure 1.3. Relative abundance of argon ions calculated for an optically thin plasma as a function of electron temperature. (From Ref. [1.20])

Recombination and collisional excitation lasers schemes both required the generation of hot, highly ionized plasma columns with a large optical length in order to achieve a significant amplification. The recombination scheme, in addition, requires rapid cooling of the plasma. The quasi-steady state implementation of a small plasma diameter is also crucial in both cases to avoid quenching of the population inversion by trapping of resonant radiation. Intensive efforts at laboratories worldwide have resulted in the

demonstration of gain at wavelengths as low as 3.5 nm to 60.8 nm in a variety of systems. However, the size, cost and complexity of the driving lasers have hampered the widespread use of soft x-ray lasers. Further progress in this field largely depends on the development of lower cost, higher efficiency table-top x-ray lasers. With this motivation significant efforts have been devoted in the past several years to the exploration of soft x-ray laser excitation schemes that make use of table-top laser drivers [1.15-1.18]. Important progress has been made in this direction through the application of the prepulse technique to collisional lasers, the development of transient inversion lasers, and the introduction of optical field ionized schemes [1.16-1.18].

Alternatively, our group has opened a new route to the development of compact tabletop amplifiers with the demonstration of large soft x-ray amplification in a plasma column generated in a capillary geometry by a fast electrical discharge [1.2]. This new excitation scheme [1.19] has significantly increased the simplicity and wall plug efficiency of ultra short-wavelength lasers.

1.3. Capillary discharge pumped soft x-ray lasers

As an alternative to laser, axial Z-pinch discharges have been proposed as drivers for soft x-ray lasers due to their higher overall energy conversion efficiency and possibility of creating elongated plasma columns with the characteristics required for x-ray lasing [1.20]. However, despite many efforts, there was no clear indication of significant gain in pulse power discharges prior to the experiments conducted at our laboratory in 1994. A key issue related to this failure is the inherent instabilities associated with Z-pinch plasmas. A discharge pumped scheme capable of overcoming

these difficulties was proposed at CSU in 1988 [1.19]. It involved the creation of highly ionized plasma columns by using fast capillary discharges. Several inherent characteristics of capillary discharges make them attractive for extreme ultraviolet and soft x-ray amplification: highly uniform initial conditions, high power density deposition, large length-to-diameter ratio, and the possibility of creating small-diameter plasma columns.

1.3.1. Capillary Discharge plasmas

Capillary discharges have been initially studied as sources of soft x-ray radiation for spectroscopy, x-ray lithography and microscopy [1.21, 1.22]. In 1988 these discharges have been proposed as gain medium for compact, high efficiency soft x-ray lasers [1.19].

The possibility of obtaining soft x-ray amplification by plasma recombination in a capillary discharge has motivated several experimental studies of the soft x-ray emission from evacuated polyacetal and polyethylene capillaries that are 0.5-1 mm in diameter [1.23-1.28]. Spectra from these experiments are consistent with plasma temperatures in the range of 15-70 eV. In evacuated capillaries the discharge starts by surface flashover on the capillary walls, and the plasma column is composed of material ablated from the capillary walls. In discharges such as those used in the experiments mentioned above, were current pulse rise times are > 50 ns, the plasma remains significantly coupled to the walls during the course of the current pulse. Under this conditions the material injected into the plasma by wall ablation and the electron heat conduction from the plasma column to the walls limits the temperature to relatively low values. An increase of the excitation current does not necessarily result in a significantly higher plasma temperature,

as an increase in the discharge energy results in more ablated material and higher plasma densities. In effect, high current pulses (500 kA) of 300 ns rise time injected through narrow capillary channels have created cold (Te = 10 eV), high density plasmas which have been used for the study of transport coefficients in partially degenerated, strongly coupled plasmas [1.29].

Higher temperatures in evacuated capillaries can result from utilizing a very fast rise current pulse to limit the amount of material ablated from the capillary walls, before the magnetic field created by the current pulse detaches the plasma from the walls. High temperature plasmas, with emission from FVIII and FIX have been reported to result from the excitation of 1 mm diameter evacuated Teflon capillaries with 120 kA current pulses having a fast (< 10 ns) rise time [1.30].

Experiments designed to study the generation of argon plasmas for soft x-ray amplification were conducted utilizing the fast capillary discharge setup show in fig. 1.4 at Colorado State University [1.5]. These experiments made use of a high voltage fast pulse generator which produces currents pulses having a 10 % to 90 % rise time of 13 ns and a full width half maximum (FWHM) of 28 ns. In this setup the capillary is in the axis of a 3 nF circular parallel plate capacitor containing ethylene glycol as the dielectric The capacitor was charged by a seven stage, 700 kV Marx generator. The pulse generator utilized in these experiments was designed to also produce a preionization pulse with a current of 20-70 A and a duration of approximately 2 μs immediately preceding the fast discharge pulse. With this generator, studies were conducted in polyacetal and Teflon capillaries having lengths of either 1 or 5 cm and diameters of 1.5 and 2.5 mm.

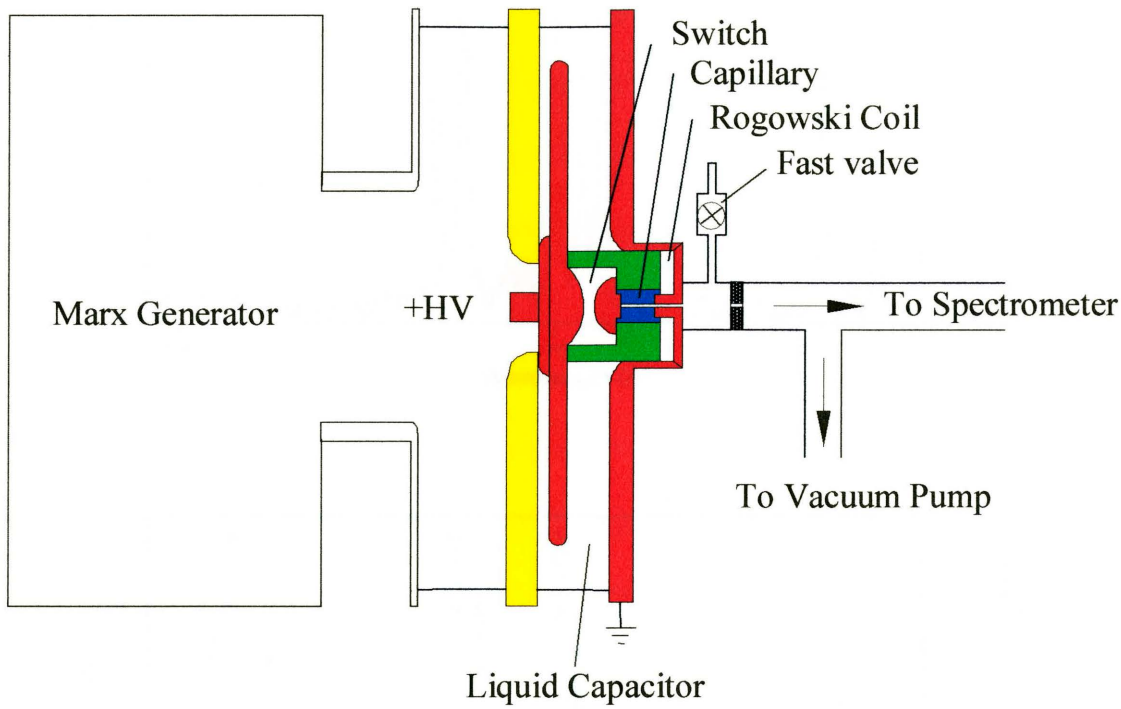

Figure 1.4. Schematic diagram of the pulse generator and capillary discharge setup utilized by Rocca et al. [1.5].

Soft x-ray spectra (fig. 1.5a) from argon plasma obtained with this discharge were reported to be similar to those of plasmas generated by > 1 MA current implosions in large pulsed power machines (fig. 1.5b) [1.31]. For a 55 kA discharge in argon at about 750 mTorr an electron density of $\cong 5 \times 10^{18}$ cm^{-3} and an electron temperature up to 170 eV were estimated to occur in the hot region of the plasma. Soft x-ray pinhole images showed that the current pulse rapidly compressed the plasma to form plasma columns 200-300 μm in diameter.

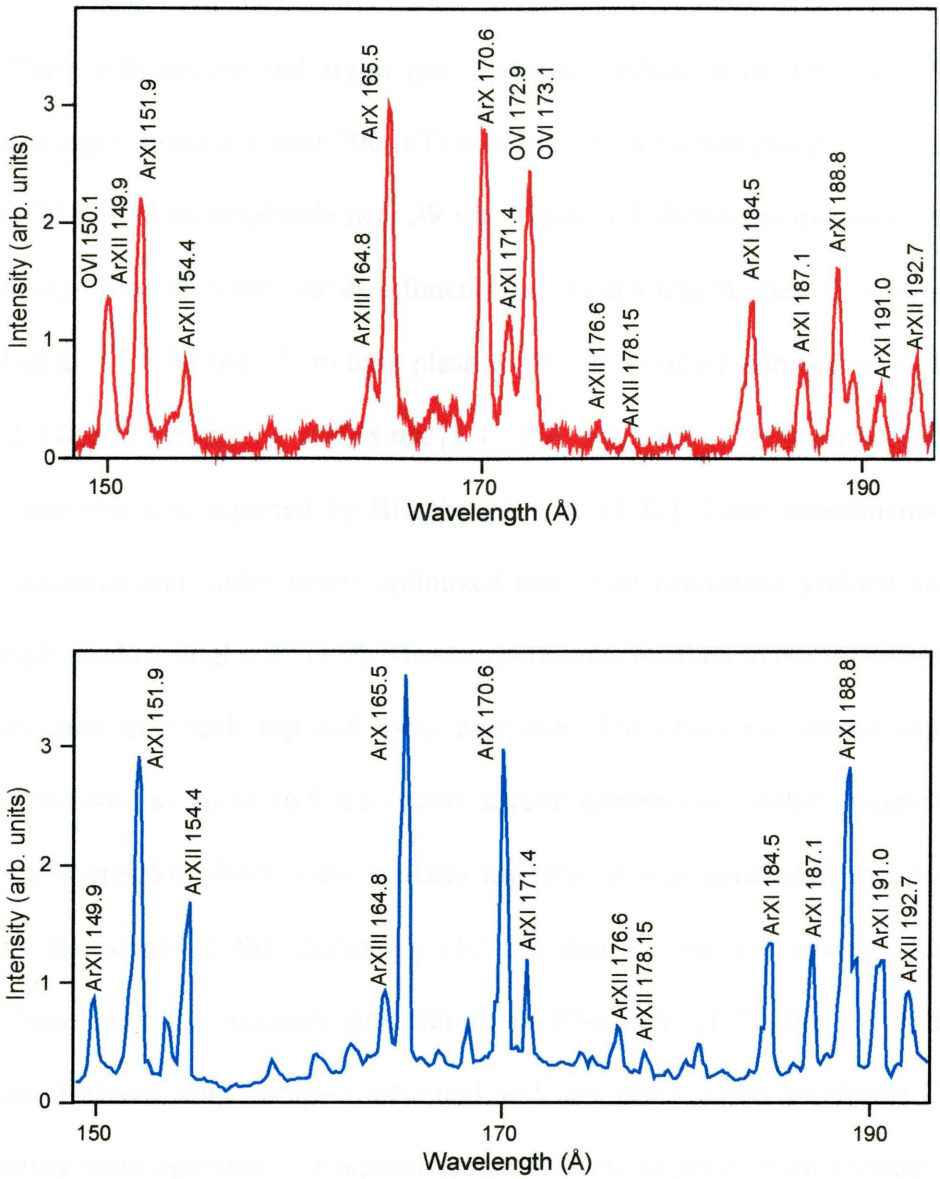

Figure 1.5.Comparision between two time resolve spectrum from: a) a 2.5 mm diameter capillary exited by a 43 kA current pulse after Rocca et al. [1.5] and b) one obtain in the Gamble II Generator (NRL) with a current pulse of 1 MA by Burkhalter et al. [1.31].

1.3.2. Capillary Discharge Soft X-ray Lasers

The first observation of large soft x-ray amplification in a discharge-created plasma was realized in 1994 [1.1] in the 3s $^1P_1{}^0$-3p $^1S_0$ line of Ne-like Ar at 46.9 nm using the fast capillary setup illustrated in fig 1.5. In that initial experiment, argon plasma

columns were generated in 4 mm diameter polyacetal capillary channels of up 12 cm in length filled with pre-ionized argon gas. Large amplification in ArIX at 46.9 nm was realized at argon pressures near 700 mTorr excited by a current pulse with a half-period of about 70 ns and an amplitude near 39 kA. Figure 1.6 shows the measured increase of the intensity of the 46.9 nm line as a function of plasma length; they show a gain-length product of gl = 7.2 for the 12 cm long plasma column. A small gain was also observed in the J = 2-1 line of Ne-like Ar at 69.8 nm [1.4]. The existence of small amplification in the J = 2-1 line was also reported by Hildebrand et al. [1.32]. Later experiments in longer plasma columns and under better optimized discharge conditions yielded an effective gain-length product of gl = 27 [1.2]. These experiments resulted in the first observation of gain saturation in a table-top soft x-ray amplifier. The optimum plasma condition for lasing in the Ne-like Ar at 46.9 nm occurs several nanoseconds before stagnation, when the first compression shock wave reaches the axis. It was concluded that lasing takes place on the slope of the increasing electron density when it reaches values near $3\text{-}9\text{x}10^{18}\,\text{cm}^{-3}$ and the electron temperature is 60-80 eV [1.2]. Based on the results summarized above, very compact saturated 46.9 nm lasers were developed [1.33-1.34] and recently were operated at a repetition rate of 7 Hz to produce an average energy of 135 μJ, corresponding to an average power of 1 mW [1.35].

The capillary discharge results in the Ne-like Ar laser were extended to the Ne-like S, with the demonstration of gain-length products of 7.5 in the $3s\ ^1P_1{}^0\text{-}3p\ ^1S_0$ line at 60.8 nm [1.3]. This experiment demonstrated that large amplifications in discharge-created plasmas could be also obtained in elements that are solid at room temperatures. To obtain amplification the original configuration show in figure 1.5 was

modified to allow the injection of sulfur vapor into the capillary through the axial hole of the ground electrode.

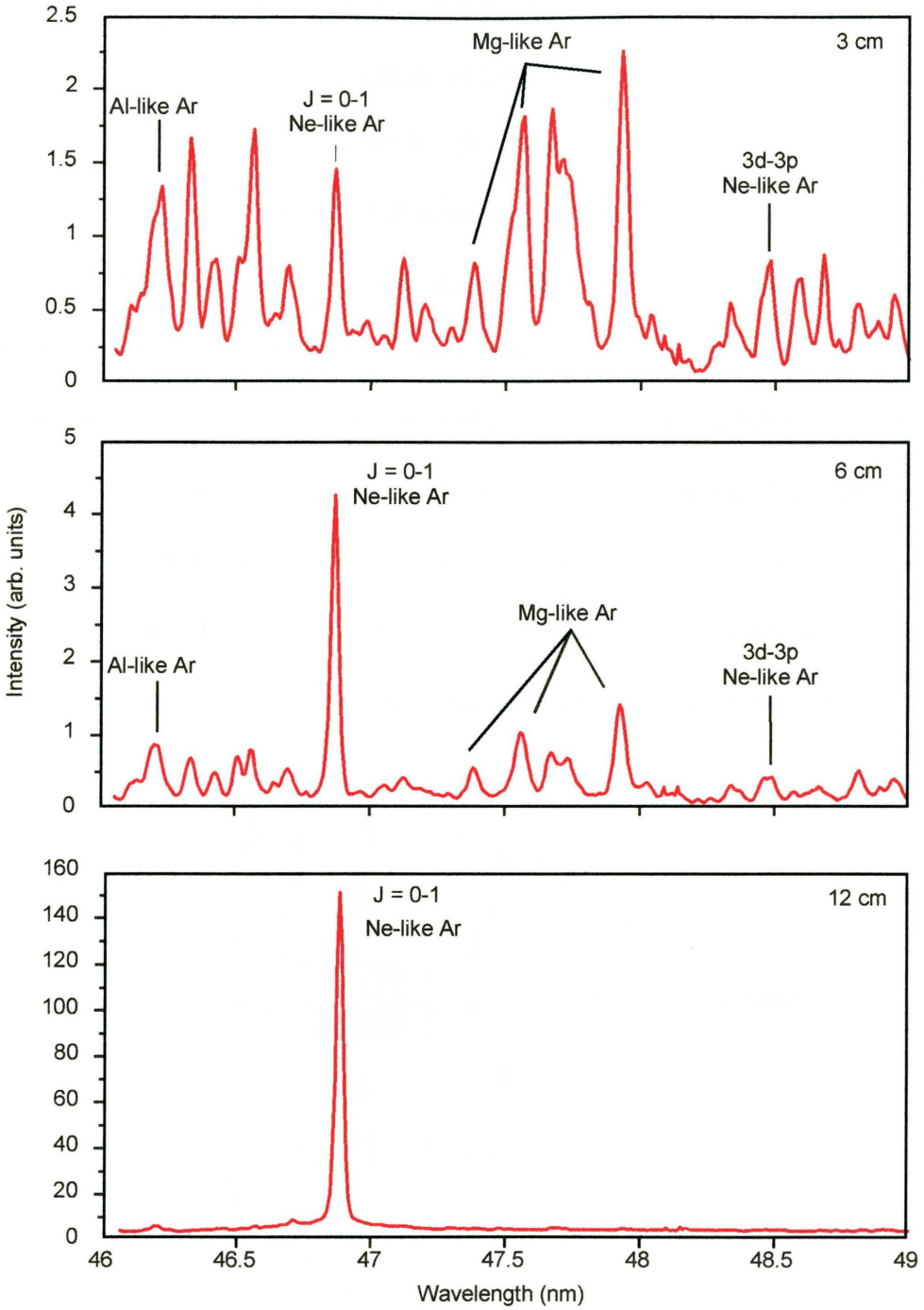

Figure 1.6. Variation of the intensity of the spectral lines in the neighborhood of 48 nm as a function of capillary length [1.1].

As shown in figure 1.7. The vapor was produced by ablating the wall of a 5 mm in diameter 2 cm long sulfur channel with a current pulse delivering 200 J in about 50 μs. At the time of lasing, which for this experiment is observed to occur near the time of maximum current, the electron density and temperature in the gain region are computed to be about 2-3x10^{18} cm^{-3} and 60-80 eV, respectively [1.3]. The optimum excitation current was found to be a 38 kA with a semi-period of 71 ns.

Besides these very successful results obtained utilizing the collisional excitation scheme, a number of studies have been conducted at several laboratories [1.24, 1.23, 1.36] to attempt the demonstration of amplification following three-body recombination of a capillary plasma. Reports of observation of amplification in the Balmer α transition of H-like carbon [1.26, 1.36] and the observation of anomalous line intensity ratio indicative of gain [1.27] have appeared in the literature. However, the amplification reported has been small, and more important it has not been reproducible.

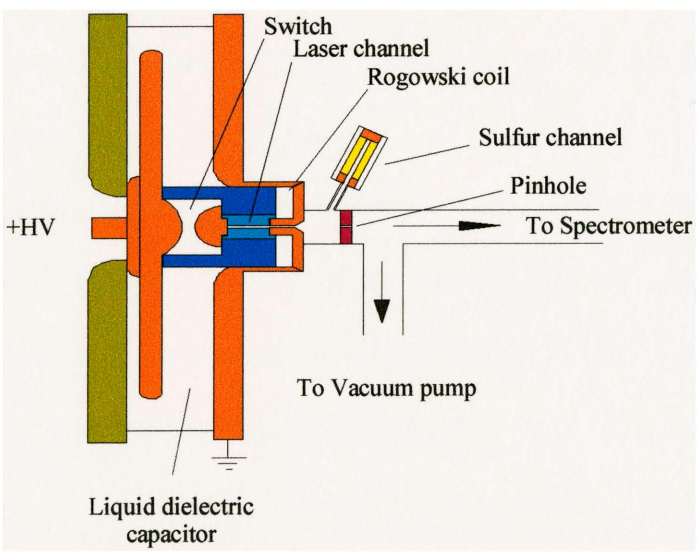

Figure 1.7. Schematic diagram of the discharge showing the relative position of the sulfur discharge respect to the laser channel after Tomasel et al. [1.3].

Small amplification of extreme ultraviolet radiation at wavelength about 50 nm in a recombining z-pinch plasma has also been reported [1.37]. Discharge currents of 40 kA with rise times of about 100 ns were used to produce amplification in the 4f-3d and 4d-3p transitions of the Li-like O. The gain-length products were determined to be 2.5 (4f-3d) and 2.2 (4d-3p), corresponding to electron temperatures of $\approx$ 50 eV and electron densities of 3-5x10^{19} cm^{-3}. More recently gain was also reported in Li-like Ne at 29.2 nm [1.38] in an experiment that utilized a discharge pulse of 80 kA to excite 4-6 mm diameter ceramic capillaries filled with Ne. The maximum gain length product for the 29.2 nm 4f-3d transition was determined to be gl = 3$\pm$0.5. However these results were not confirmed by gain-length measurements.

1.4. Summary

In summary, capillary discharge excitation of the lasing medium is among the most promising schemes for the development of table-top soft x-ray lasers. This excitation scheme has shown its potential for increasing the simplicity and the wall-plug efficiency of ultra-short-wavelength lasers.

This dissertation addresses topics related to the important issue of the extension of capillary discharge soft x-ray lasers to shorter wavelengths. It focuses in the generation of hotter and denser plasma columns with the characteristics necessary for soft x-ray amplification at wavelengths shorter than 46.9 nm.

1.5. References

1.1. J.J. Rocca, V. N. Shlyaptsev, F. G. Tomasel, O. D. Cortazar, D. Hartshorn and J. L. A. Chilla, "Demonstration of a Discharge Pumped Table-Top Soft-X-Ray Laser", *Phys. Rev. Lett.* **73**, pp. 2192-2195, 1994

1.2. J. J. Rocca, D. P. Clark, J. L. A. Chilla and V. N. Shlyaptsev, "Energy Extraction and Achievement of the Saturation Limit in a Discharge-Pumped Table-Top Soft X-ray Laser Amplifier", *Phys. Rev. Lett.* **77**, pp. 1476-1479, 1996.

1.3. F. G. Tomasel, J.J. Rocca, V. N. Shlyaptsev and C. D. Macchietto, "Lasing at 60.8 nm in Ne-like sulfur ions in ablated material excited by a capillary discharge", *Phys. Rev. A* **55**, pp. 1437-1440, 1997.

1.4. J.J. Rocca, F. G. Tomasel, M. C. Marconi, V. N. Shlyaptsev, J. L. A. Chilla, B. T. Szapiro and G. Giudice, "Discharge –pumped soft-x-ray laser in neon-like argon", *Phys. Plasmas* **2**, pp2547-2554, 1995.

1.5. J.J. Rocca, O. D. Cortazar, B. T. Szapiro, K. Floyd and F. G. Tomasel, "Fast-discharge excitation of hot capillary plasmas for soft-x-ray amplifiers", *Phys. Rev. E* **47**, pp. 1299-1304, 1993.

1.6. J. J. Gonzalez, M. Frati, J. J. Rocca and V. N. Shlyaptsev, "First experimental results of a very high power density capillary discharge plasma", *Proc. Of the X-ray Lasers Conf.*, pp. 163-166, 1998.

1.7. G. A. Gudzenko and L. A. Shelepin, *Zh. Eksp. Teor. Fiz.* **45**, pp. 1445, 1963. [*Sov. Phys.* **JETP 18**, pp. 998, 1964.]

1.8. M. A. Dugay and P. M. Rentzepis, *Appl. Phys. Lett.* **10**, pp. 350, 1967.

1.9. R. C. Elton, "Extension of 3p-3s ions lasers into the vacuum ultraviolet region", *Appl. Opt.* **14**, pp. 97-101, 1975.

1.10. A. V. Vinogradov, I. I. Sobel'man and E. A. Yukov, "Population-inversion at transitions in Neon-like ions", *Kvantovaya Elektronica* **4**, pp. 63-68, 1977.

1.11. A. V. Vinogradov, I. I. Sobel'man and E. A. Yukov, "Feasibility of a far ultraviolet laser utilizing transitions of multicharge ion in inhomogeneous plasma", *Kvantovaya Elektronica* **2**, pp. 105-113, 1975.

1.12. D. L. Matthews, P. L. Hagelstein, M. D. Rosen, M. J. Eckart, N. M. Ceglio, A. U. Hazi, H. Medecki, B. J. MacGowan, J. E. Trebes, B. L. Whitten, E. M. Campbell, C. W. Hatcher, A. M. Hawryluk, R. L. Kauffman, L. D. Pleasance, G. Rambach, J. H. Scofield, G. Stone, and T. A. Weaver, "Demonstration of a soft x-ray amplifier", *Phys. Rev. Lett.* **54**, pp.110-113, 1985.

1.13. S. Suckewer, C. H. Skinner, D. Kim, E. Valeo, D. Voorhees, and A. Wouters, "Divergence measurements of soft x-ray laser beam", *Phys. Rev. Lett.* **8**, pp. 1004-1007, 1986.

1.14. H. R. Griem, "Principles of Plasma Spectroscopy", *Cambridge University Press*, Cambridge 1997.

1.15. J. Dunn, A. L. Osterheld, R. Shepherd, W. E. White, V. N. Shlyaptsev, and R. E. Stewart, "Demonstration of X-Ray Amplification in Transient Gain Nickel-like Palladium Scheme", *Phys. Rev. Lett.* **80,** pp. 2825-2828, 1998.

1.16. D. Korobin, C. H. Nam, S. Suckewer and Golstov, "Demonstration of Soft X-Ray Lasing to Ground State in LiIII", *Phys. Rev. Lett.* **77**, pp. 5206-5209, 1996.

1.17. B. E. Lemoff, G. Y. Yin, C. L. Gordon III, C. P. J. Barty and S. E. Harris, "Demonstration of a 10 Hz, femtosecond-pulse-driven XUV laser at 41.8 nm in XeIX", *Phys. Rev. Lett.* **74**, pp. 1574-1577, 1995.

1.18. P. V. Nickles, V. N. Shlyaptsev, M. Kalachnikov, M. Schnürer, I. Will, and W. Sandner, "Short Pulse X-Ray Laser at 32.6 nm Based on Transient Gain in Ne-like Titanium", *Phys. Rev. Lett.* **78,** pp. 2748-2751, 1997.

1.19. J. J. Rocca, D. C. Beethe, and M. Marconi, "Proposal for soft-x-ray and XUV lasers in capillary discharges", *Opt. Lett.* **13**, pp. 565-567, 1988.

1.20. K. W. Hill, M. Bitter, D. Eames, S. von Goeler, N. R. Sauthoff, and E. Silver, "Low energy x-ray emission from magnetic fusion plasmas", *AIP Conference Proceedings* **75,** D. T. Atwood and B. L. Henke, eds., pp.8-24, 1981.

1.21. P. Bogen, H. Conrads, G. Gatti and W. Kohlhaas, *J. Opt. Soc. Am.* **58**, pp. 203, 1968.

1.22. R. A. McCorkle," High-power sliding-spark capillary discharge in vacuum: variation and applications", *Appl. Phys. A* **26**, pp. 261-270, 1981.

1.23. C. Steden and H. J. Kunze, "Observation of gain at 18.22 nm in the carbon plasma of a capillary discharge", *Phys. Lett. A* **151**, pp. 534-537, 1990.

1.24. C. A. Morgan, E. J. Iglesias, H. R. Griem, H. J. Kunze and R. C. Elton, "A capillary discharge experiment for the investigation of possible gain in the Hα line of CVI", *IEEE Nuclear & Plasma Sciences Soc. Publ. by IEEE*, pp. 162, 1991.

1.25. J. J. Rocca, M. Marconi and F. G. Tomasel, "Study of the soft-x-ray emission from carbon-ions in a capillary discharge", *IEEE J. Quantum Electron.* **29**, pp. 182-191, 1993.

1.26. J. J. Rocca, M. Marconi, B. T. Szapiro and J. Meyer, "Experiments on soft x-ray laser development in a tabletop capillary discharge", *Proc. SPIE* **1551**, pp.275-281, 1991.

1.27. C. A. Morgan and H. R. Griem and R. C. Elton, "Spectroscopic measurements of electron density and temperature in polyacetal-capillary-discharge plasmas', *Phys. Rev. E* **49**, pp. 2282-2290, 1994.

1.28. R. L. Shepherd, D. R. Kania and L. A. Jones, "Measurement of the resistivity in a partially degenerate, strongly coupled plasma", *Phys. Rev. Lett.* **69**, pp. 1278-1281, 1988.

1.29. S. M. Zakarov, A. A. Kolomenskii, S. A. Pikuz and A. I. Samokhin, *Pis'ma Zh. Tekh. Fiz.* **6**, pp. 1135, 1980. [*Sov. Tech. Phys. Lett.* **6**, pp. 486, 1980].

1.30. P. G. Burkhalter, G. Mehlmann, F. C. Young, S. J. Stephanakis, V. E. Scherrer and D. A. Newman, "Soft x-ray emission from gas puff implosion", *J. Phys.-Paris* **47**, pp. 247-252, 1986.

1.31. A. Hildebrand, A. Ruhrmann, S. Maurmann and H. J. Kunze, "Amplified spontaneous emission on the J=2->1,3p-3s transition of neonlike argon in a capillary discharge", *Phys. Lett. A* **221**, pp. 335-338, 1996.

1.32. C. D. Macchietto, B. R. Benware and J. J. Rocca, "Generation milli-jule level pulses at 4 Hz repetition rate with a capillary discharge table-top soft-x-ray laser", *Opt. Lett.* (in press).

1.33. B. R. Benware, C. H. Moreno, D. J. Burd, and J. J. Rocca, "Operation and output pulse characteristics of an extremely compact capillary-discharge tabletop soft-x-ray laser", *Opt. Lett.***22**, pp. 796-798, 1997.
1.34. B. R. Benware, C. D. Macchietto, C. H. Moreno, and J. J. Rocca, "Demonstration of a High Average Power Tabletop Soft X-Ray Laser", *Phys. Rev. Lett.* **81**, pp. 5804-5807, 1998.
1.35. Hyun-Joon Shin, Dong-Eon Kim, and Tong-Nyong Lee, "Soft-x-ray amplification in a capillary discharge", *Phys. Rev. E* **50**, pp. 1376-1382, 1994.
1.36. T. Wagner, E. Eberl, K. Frank, W. Hartmann, D. H. H. Hoffmann, and R. Tkotz, "XUV amplification in a recombining z-pinch plasma", *Phys. Rev. Lett.* **76**, pp. 3124-3127, 1996.
1.37. T. Böß, W. Neff, T. Boboc, F. Weigand, R. Bischoff and H. Langhoff, "Optical gain for the Ne VIII 4-3 transition by capillary discharge pumping", *J. Phys. D* **31**, pp. 2472-2478, 1998.

CHAPTER 2

HIGH POWER CAPILLARY DISCHARGE SET UP

2.1. Introduction

The principal function of many pulsed high power systems is to accept energy from a low voltage source over a relatively long period of time and at a modest current level, and subsequently deliver that energy with maximum efficiency, at high voltage and current levels in a very short time. This energy is usually delivered to some kind of load, in our case a capillary plasma column. The primary requirement for these systems is to maintain maximum efficiency in the transfer and conversion of the stored energy from the pulser to the load.

Maximum energy can be transferred to the load in minimum time when an impedance match is maintained between the power source and the load. In our application we have chosen to supply the load with a short pulse delivered from a constant impedance source. This objective can be met by the use of either distributed and/or lumped-constant pulse forming networks. Certain requirements must be satisfied: namely, the electric storage media should exhibit low volume and surface leakage during the time of charging, and it should withstand very high electric fields before the onset of

output discharge. High energy density storage is important to realize a relatively compact device (this dictates the use of high dielectric constant materials for energy storage). No less important are the geometry considerations of the pulsed power package. Besides being suitable for efficient energy storage and permitting effective coupling at the proper impedance level to the load, it should be reliable, and it should have an efficient method of switching the energy from the stressed dielectric to the load.

It has long been recognized that switching problems are among the most severe encountered in the design and development of low-impedance, fast-pulse power sources. Switching energy from the pulser to the load should introduce minimum resistive loss, inductance and distortion. Switches should exhibit long life, or at least should be easy to service. Furthermore, the energy delivered by the pulse generator must be coupled to a capillary load that is part of a vacuum system. As discussed later in this thesis, this frequently poses design problems because of conflicting requirements for impedance matching, voltage breakdown, instrumentation requirements, etc.

2.2. High Power Capillary Discharge Setup

After evaluating the advantages and drawbacks of different approaches to the pulse generator design the three-stage compression scheme show in figure 2.1 was chosen. This high voltage pulse generator is able to generate current pulses having 10 % to 90 % rise times of about 10 ns, and a full width half maximum (FWHM) of 20 ns when 1 cm long capillary channels are used as a load. Discharge pulses with peak currents exceeding 200 kA were obtain over 3.3 mm diameter capillary loads under normal operation conditions (fig. 2.2).

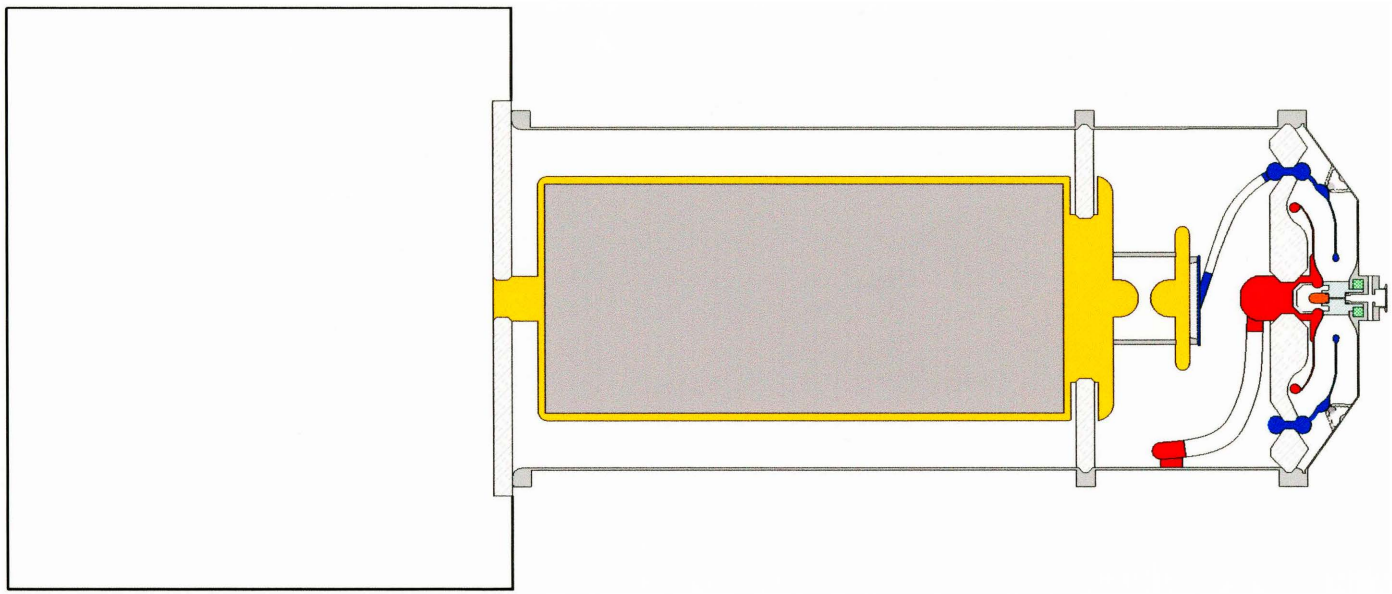

Power Supply 30 mA DC	Marx Stage 10 kA Peak 700 ns Rise	Coaxial Water Capacitor Stage 80 kA Peak 75 ns Rise	Main Spark Gap Switch	Blumlein Stage 200 kA Peak 10 ns Rise

Figure 2.1. Schematic illustration of the pulse compression scheme to produce high power electrical pulses by successive transfer of energy.

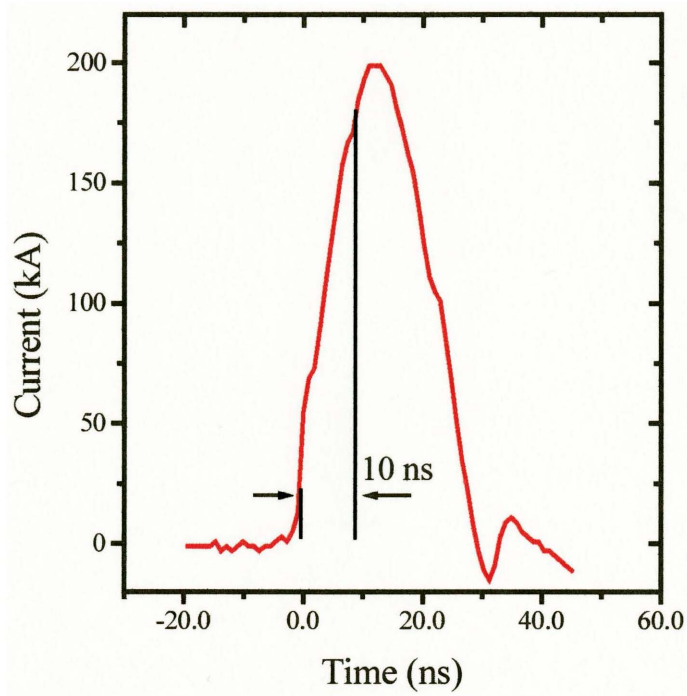

Figure 2.2. Typical current pulse characteristics obtain over a 1 cm long capillary load.

This generator was built on the basis of the water-Blumlein-line technology and designed for the production of hot, dense capillary plasmas. The block on the leftmost of the figure 2.2 represents an eighth stage Marx generator, which serves as the initial energy storage medium and a voltage multiplier. When fully charged, it generates pulses with a peak voltage of 800 kV. The second stage is a coaxial water capacitor consisting of two coaxial cylinders with a single spark gap connected at the end of the inner cylinder. The water capacitor serves as an intermediate compression stage, as the voltage pulse generated by the Marx generator is in the microsecond range and is excessive slow to be utilized to charge the final stage. The final stage is a radial Blumlein transmission line consisting of three circular plates with an array of spark gap switches connected between the middle plate and the outer plate. It is connected to the water capacitor through the spark gap switch and a series damping resistor.

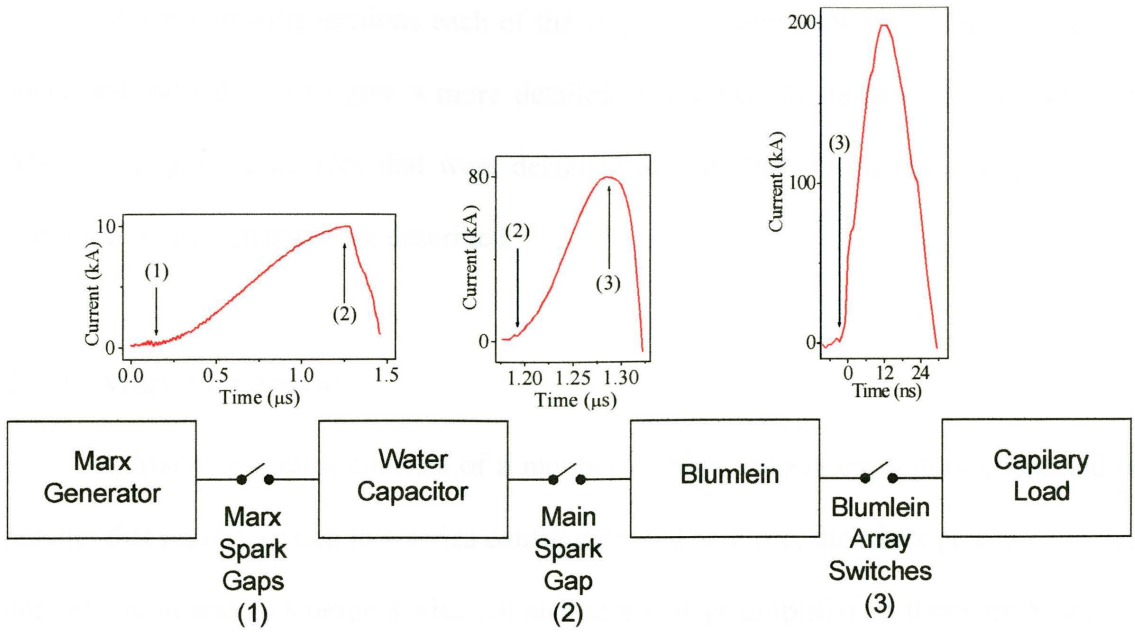

Figure 2.3. Block diagram showing the operating principle and the observed outputs of the current generator. The arrows indicate the relative time at which the different switches are closed.

The block diagram shown in fig. 2.3 qualitatively describes the basic principle of operation of the generator and shows typical output pulses. Upon firing the Marx generator, a voltage pulse of about 800 kV peak, 700 ns rise is generated. This pulse charges the water capacitor. When the water capacitor is nearly fully charged, it is discharged through the SF_6 switch, described herein as the main spark gap switch. The faster pulse that is formed charges the Blumlein in approximately 75 ns. Immediately after, the array of switches of the Blumlein are triggered, generating a very fast, high peak current pulse through the capillary load.

Before this current pulse reaches the capillary, plasma must be pre-ionize. The pre-ionization is achieved with a low amplitude slow current pulse. This technique helps the formation of a uniform plasma column suitable for laser amplification. The pre-ionization pulse is generated by an auxiliary discharge that is fires 10 μs before the main discharge.

In the following sections each of the stages that constitute the pulse generator is addressed individually to give a more detailed description of its design and operation. Also the diagnostic devices that were designed and utilized during the debugging and operation of the generator are described.

2.2.1. Marx Generator

A Marx Generator consists of a number of high voltage capacitors connected in parallel that rapidly switch to a series configuration. Therefore, the Marx generator serves not only as an energy storage device but also as a voltage amplifier. If there are N stages, in principle the output voltage can be N times the original voltage.

The Marx generator circuit is illustrated in fig 2.4. It consists of eight capacitor stages, dc charged to as much as 100 kV, and eight spark gaps. Those are switched to produce the required output pulse voltage. Each capacitor stage is composed of two 75 kV capacitors connected in series. The capacitors are nominally 800 nF units and each stores an energy of 1 kJ at 50 kV, giving a total energy of 2 kJ per stage and 16 kJ for the entire bank.

The generator spark gaps are pressurizing gas (synthetic air) switches equipped with a mid-plane irradiation triggering. The irradiated spark gap switch (fig. 2.5) utilizes a small spark source in the center trigger electrode. A trigger pulse applied to this type of spark-gap source generates a small plasma on the center electrode region, creating an ultra violet source that irradiates the gas between the two main electrodes. This irradiation generates free electrons between one or both main electrodes and the center

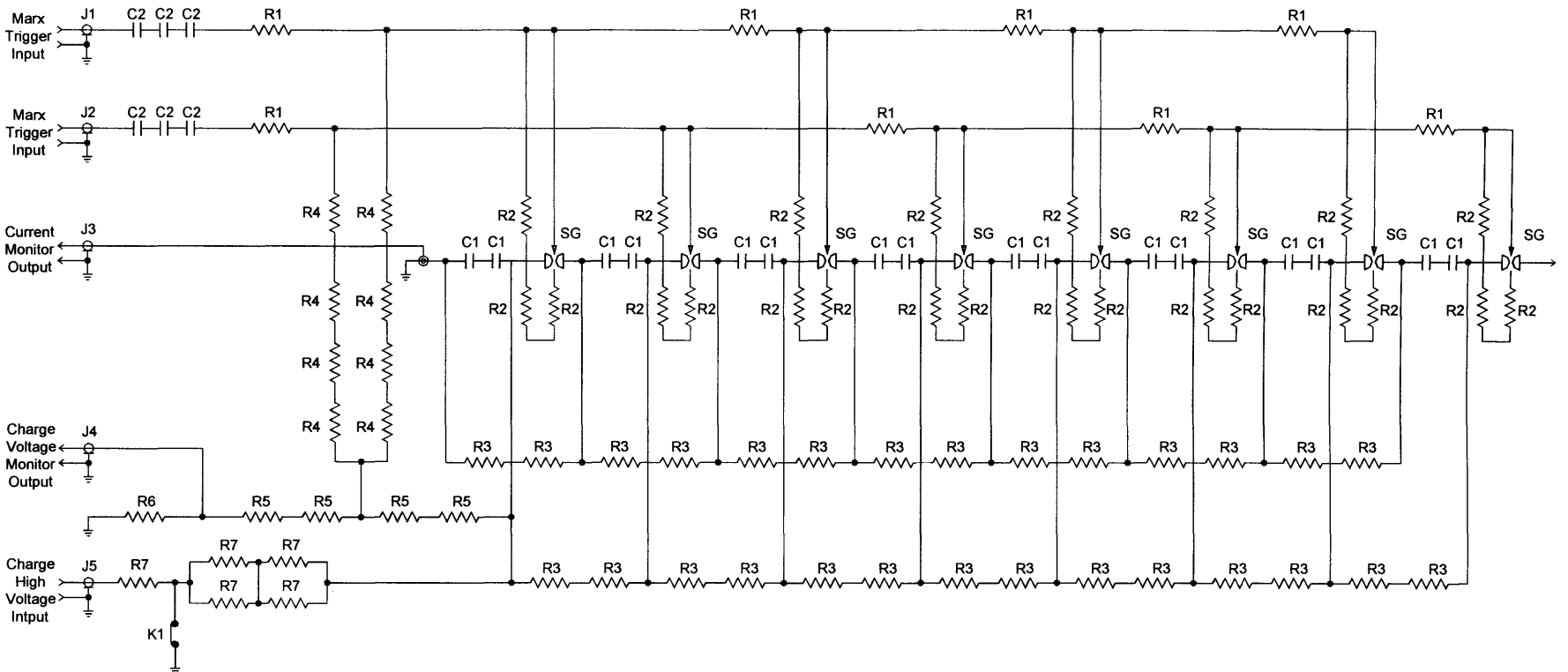

Figure 2.4. Circuit diagram of the Marx Generator. R1 = 130 Ω, R2 = 5 MΩ, R3 = 2 kΩ, R4 = 510 kΩ, R5 = 100 MΩ, R6 = 8 x 47 kΩ, R7 = 100 kΩ, C1 = 0.8 μF, C2 = 2 nF, SG = Irradiated midplane spark gap, K1 = High voltage grounding relay.

trigger electrode, thus ensuring a more controlled over-voltage breakdown between the electrodes. This triggering approach is generally relied upon to reduce jitter.

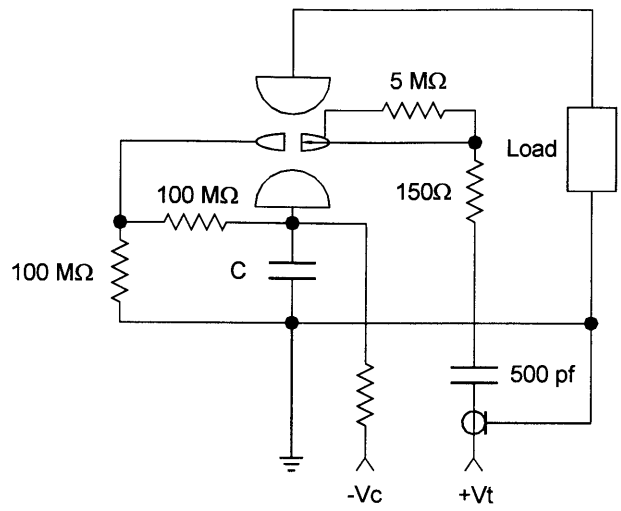

Figure 2.5. Schematic diagram of the configuration and typical circuit arrangement utilizes to operate an irradiated midplane spark gap.

During DC charging of the Marx, the mid-plate plane electrodes are resistively biased at V/2, where V is the voltage drop over the switch main electrodes (fig. 2.5). Thus for this condition, there exists no field enhancement at the mid-plane electrode. However, when triggered, the mid-plane electrodes are electrically displaced from their mid-voltage value and the electric field increases to a large value. Thus the gas in the high field region rapidly breaks down with subsequent arc closure to one of the main electrode and then to the other main electrode, thereby completing the circuit. The break down processes are enhanced by the ultra violet radiation emitted in the irradiation pin, that reduces the closure jitter of the switch.

The Marx generator is triggered with a 100 kV trigger generator (Maxwell Inc.) provided with two output cables. The two trigger generator output cables are capacitively

coupled to each of the Marx trigger chains. Each chain fires half of the Marx spark gaps in an interlace manner.

The Marx is crowbarred by means of a triggered, pressurized gas (SF_6) spark gap. Because the crowbar switch must withstand the full Marx output voltage (800 kV) a trigatron-type spark gap is utilize. This type of switch (fig. 2.6) has an insulated trigger pin inserted along the centerline of the ground electrode. A trigger pulse applied to this pin forms a discharge between the trigger pin and the main electrode, producing a conducting plasma that expands into the region of electric field between the two main electrodes increasing the electric field until breakdown occurs. Like the Marx switches the crowbar switch pressure is monitored and adjusted from a control rack.

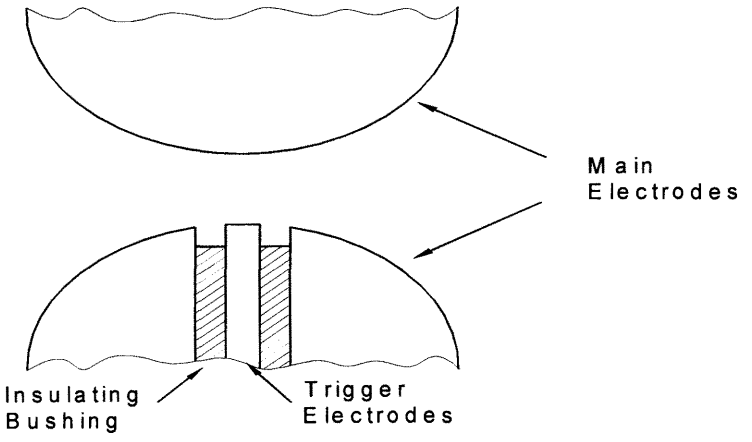

Figure 2.6. Schematic of a trigatron spark gap.

The equivalent circuit of the Marx generator during production of the output pulse is illustrated in fig. 2.7. The inductance Ls in fig. 2.7 is the Marx generator equivalent stray series inductance. This inductance is associated principally with the spark gaps and their connections to the individual capacitor stages. The lumped resistor Rc in the crowbar circuit is added to dissipate the Marx energy and limit the energy storage

capacitor reversal after the Marx is crowbarred. Ll is a charging inductance added to avoid the discharge of the water capacitor during the crowbaring of the Marx, without appreciably reducing the voltage available to charge the water capacitor. The crowbar switch is triggered utilizing a 50 kV Maxwell trigger generator similar at the one use to trigger the Marx generator.

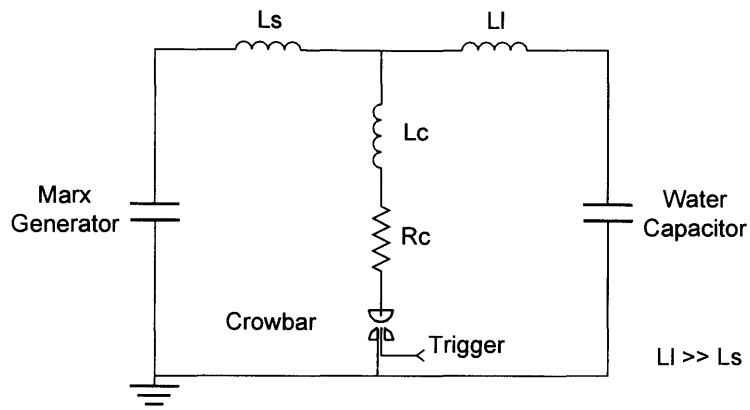

Figure 2.7. Equivalent circuit of the Marx Generator during the discharge period.

2.2.2. Water Capacitor and Main Spark Gap

As described above the Marx generator is linked to the final pulse compression stage by means of a coaxial water capacitor. This intermediate compression stage is utilized to pre-compress and amplify the Marx current pulse (fig. 2.1). The faster pulse generated by this stage allows one to charge the final stage in a shorter time, thereby diminishing the chances of electrical breakdown, and reducing the charge leakage to ground due to the finite resistance of the water dielectric utilized in the Blumlein.

The water capacitor physically consist of a stainless steel inner tube 76 cm in diameter and 1.5 m long that resides inside a 100 cm diameter cylindrical water tank. Both cylinders are held in a coaxial configuration by means of two 100 cm diameter acrylic plates. The acrylic plates also work as an interface between the water dielectric

and the insulation oil under which the Marx generator and the main spark gap are kept (fig. 2.1). This low inductance coaxial configuration provides the 26 nF capacitance required by the intermediate compression stage. It also provides sufficient electric isolation to operate at the full charging voltage of 1 MV.

When the water capacitor reaches the maximum charging voltage the Main spark gap self-breaks, connecting the water capacitor through a damping resistor (Rl) to the Blumlein transmission line. For charging purposes the Blumlein acts as two capacitors connected in parallel. Figure 2.8 shows the equivalent circuit for the two final pulse compression stages during the Blumlein charge period. Ls is the inductance associated with the switch and the electrolytic resistor, Rwc and Rwl are the water leakage resistances for the capacitor and the Blumlein respectively. Lg is the grounding inductor. Its function is to avoid an excessive floating voltage on the Blumlein line back plate during the charging stage.

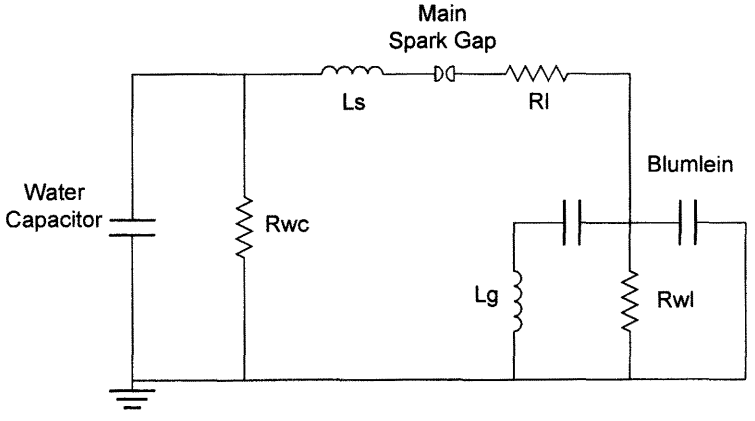

Figure 2.8. Momentary equivalent circuit during the charging of the Blumlein.

The main switch (fig. 2.1) is a gas-discharge, self-breaking, two-electrode spark gap that operates under a pressurized atmosphere of SF_6. The voltage applied across the switch increases rapidly during the water capacitor charging period, causing an

overvoltage on the switch. The SF_6 pressure in the gap is adjusted depending on the charge operation conditions, to select the voltage at which the switch will close. The damping resistor consists of two electrodes attached to a 30 cm diameter PMMA cylinder fill with a saturated copper sulfite water solution. This kind of resistor is able to handle the energy, voltage and current levels required by the design without major inconveniences.

2.2.3. Blumlein

The basic structure of a Blumlein transmission line may be conceptually considered as two simple transmission lines connected such that they are charged in a parallel configuration and discharge in series. For this reason, with proper termination, it can produce an output voltage twice as high as that of a simple transmission line. A Blumlein line can be constructed either in cylindrical or parallel-plate configurations. In parallel plate form, its basic structure involves three parallel plates arranged in the configuration shown in figure 2.9. For operation at very high voltages the space between the plates is filled with a liquid dielectric medium, such as oil or water. Between the middle (B) and lower plate (C) there is a switch to control the discharge of the line. The distance between the plates and the width of the plates is chosen to obtain the desired characteristic impedance and to maintain the electric field below the value of dielectric breakdown. The load (Z') is commonly connected between the lower (C) and the top (A) plate. The high voltage (HV) input that charges the line is fed in via the middle plate as indicate in figure 2.9.

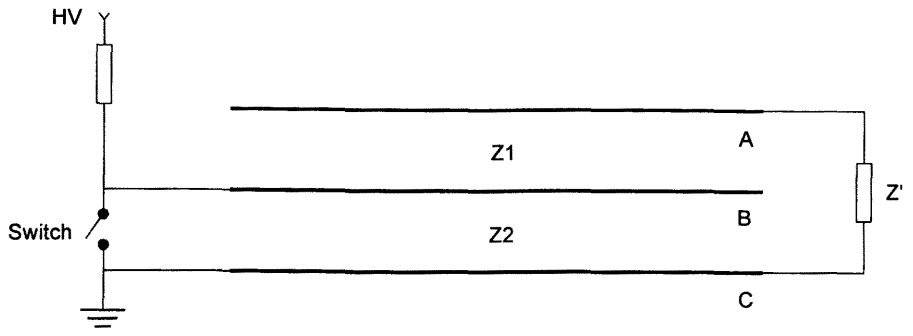

Figure 2.9. Basic structure of a Blumlein transmission line in parallel-plates configuration, A = upper plate, B = middle plate, C = lower plate; Z1, Z2 = characteristic impedance of upper and lower lines; Z' = load impedance.

In order to facilitate the discussion of its operation, let's redraw the schematic shown in fig. 2.9 into a different form in which we have Z1 = Z2 = Zo (fig. 2.10). Before the switch is closed, the system may be viewed conceptually as two charged capacitors connected in parallel configuration via a load of impedance Z'. However, no voltage drop appears over the load, since both lines are charged at the same voltage, Vo. When the switch closes, a voltage pulse of amplitude Vo is produce at the shorted end the pulse propagates along the line toward the open end and if there were no discontinuity along the line, it suffer no reflections until it reached the open end. However, the impedance Z' between plates A and C constitutes a discontinuity. When the voltage pulse reaches Z' a reflection of the pulse occurs (Vr), meanwhile a voltage pulse (Vt) is transmitted to the open line on the right. The directions of propagation of these pulses are shown in fig 2.10. In other to simplify the situation we may assume that we are under a matching load condition, that it is Z`=2Zo. At t = To = $\sqrt{(LC)} = l\sqrt{(\mu_o \varepsilon_o \varepsilon_r)}$ (where L is the transmission line total inductance and C is the transmission line total capacitance and l is the length of the line), the delay time of the transmission line, the voltage pulse Vo reaches the section

r-r', and it sees a mismatched termination of total impedance Z` + Zo or 3Zo. As a result, a reflected pulse Vr of the same polarity but with amplitude ρ_v Vo is produced, where ρ_v is the voltage reflection coefficient at the section r-r' that is equal to $\rho_v = 1/2$ for the matched load case. The total voltage across the load at this time is $V = Vo + \rho_v Vo = 3/2Vo$, of which there is a Vo/2 drop across the characteristic impedance Zo of the open line on the right and a Vo drop across the load impedance Z'. At t = 2To, the reflected pulse Vr reaches the shorted end and suffers another reflection to become Vr' = –Vo/2. Meanwhile the transmitted pulse Vt reaches the open end and suffers a reflection to become Vt' = Vo/2. At t = 3To, both Vr' and Vt' pulses reach the mismatched location. Because we are in the matched load case, i.e. Z' = 2Zo, we see that the two pulses cancel each other at that point (Vr` + Vt' = 0). Therefore, during the time interval To < t < 3To, the voltage across the load Z' is constant and equal to the input voltage Vo. For t > 3To all succeeding reflections for this line continue to cancel in a similar manner, the voltage across the load Z' drops to zero as the capacitive energy initially store in the line is now completely dissipated in the load (assuming Z' is resistive and the switch has negligible rise time). As a result, the load sees a rectangular voltage pulse of amplitude Vo and duration 2To.

In the case of a mismatched load, the pulse Vr' and Vt' would not cancel each other and some new reflection may occur at the load. Then the total voltage across the section r-r' and r-r" would have to be reevaluated, obtaining a new set of pulses Vt" and Vr". These two new pulses will bounce at the shorted and open ends of the line respectively, returning to the mismatch point. This phenomenon will repeat itself until the energy initially stored in the Blumlein is completely dissipated by the load. As a

consequence of the mismatch a wider pulse that reverses polarities several times is obtain over load.

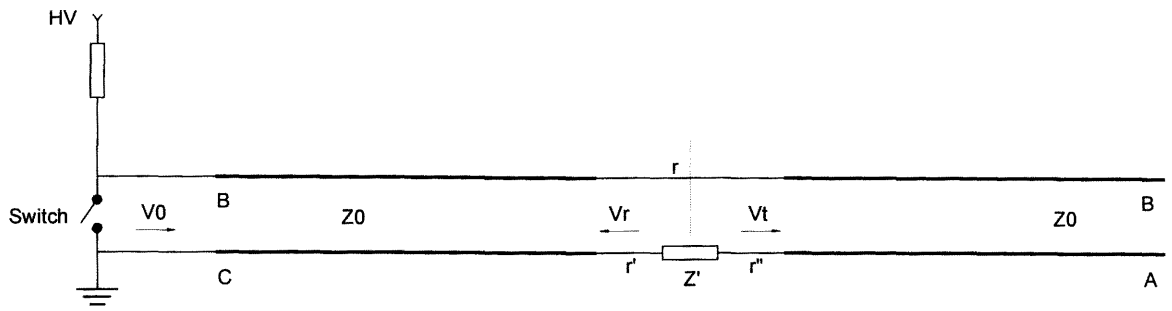

Figure 2.10. Equivalent circuit of the Blumlein line shown in fig. 2.9, with Z1 = Z2 = Z0.

In our case, the basic structure of the Blumlein previously described is modified, replacing the two uniform impedance transmission lines by two transmissions lines of radial geometry and inhomogeneous impedance (fig. 2.11). This modified Blumlein configuration is utilized, as a pulse forming line to shape the current pulse to the form required by the capillary load. The Blumlein is capable of compressing the voltage pulse from the water capacitor into a well-shaped pulse with a fast rise time and a predetermined width. As was explained before, the pulse width can be determined from the length of the Blumlein line and the dielectric constant of the liquid employed. The function of the inductor connected to the inner plate of the Blumlein (fig 2.11) is to provide a grounding path for the otherwise floating inner plate during the charging phase.

At the left end of the capillary, there is a radial self-break-down spark gap whose function is to stop the effects of the pre-pulse voltage on the capillary. Pre-pulse voltage is the result of capacitive coupling between the middle and inner plate of the Blumlein. Without the pre-pulse spark gap the voltage due to the capacitive coupling will generate a

current pulse through the capillary load. Such a pulse would pre-heat the plasma, undesirably perturbing its compression. The SF_6 gas pressure of the pre-pulse switch is properly adjusted such that it closes at the proper time, after the main voltage pulse arrives.

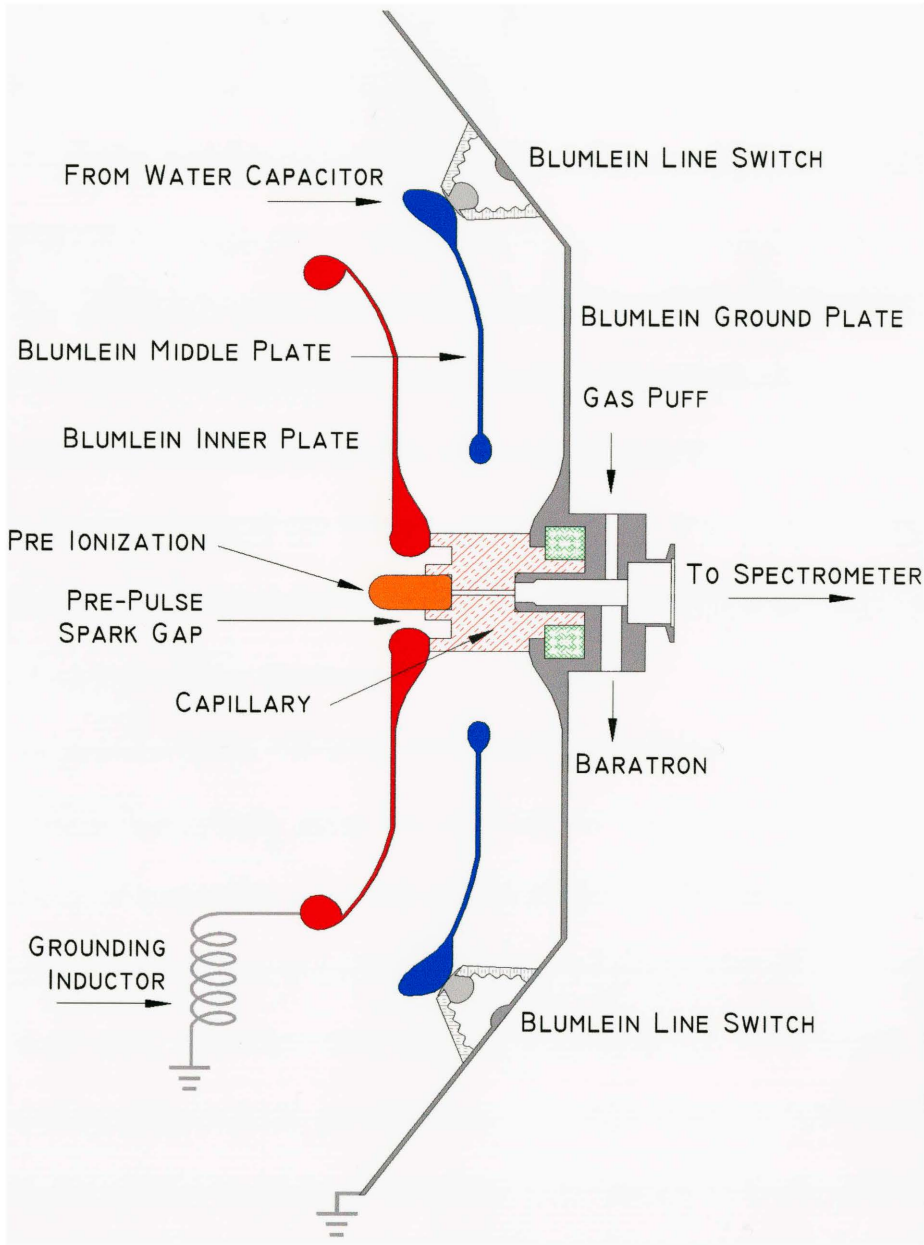

Figure 2.11. Basic structure of the radial Blumlein line.

The output pulse rise time is strongly affected by how the switching of the Blumlein is achieved. The ideal switch for a Blumlein pulser, i.e. providing a short circuit, at the line end remote to the load, would establish a low and constant impedance connection from the line to the switch, and have little or no inductance. This would require a distributed switch capable of simultaneously shorting every point of the transmission line termination. In addition it is desirable to have minimum energy dissipation in the switch, and a very long switch life, or at least a switch design that permit easy maintenance.

The switch inductance consists of the inductance of the electrodes and the switch gap itself. The effect of the switch inductance is to degrade the rise time of the current pulse, which is determined, by the L/R time constant (where L is the switch inductance and R is the impedance of the line and gap). Since the line described herein is a low impedance line (4 Ω), the switch inductance must be correspondingly low and it becomes an important parameter in the design.

To generate pulses with a fast rise time, it is also important that the switch provide a short circuit continuously along the entire end of the line. Under these conditions a voltage reversal propagates uniformly with azimuthal symmetry from the switch to the load (fig. 2.12a). However, in practice when only a finite number of localized conducting channels are used, a non-symmetric propagation is obtained. For example, shorting the transition line of figure 2.12b at points A and B results in a perturbation, which will not be felt at point D until a period of time equal to the single transit time between point A and D has passed. Thus, following switching, a reversal wave develops and begins to propagate from A and B toward C, but it will not begin to propagate from D toward C

until a later time. Thus an asymmetrical wave propagates down the line towards the load. Therefore, the resulting pulse that the load experiences is not a step function (assuming a depreciable switch inductance) but a ramp, having a rise time that is related to the transit time from A to D. Therefore, it becomes important to switch as many points around the periphery of the Blumlein as possible. On the other hand having a number of switches big enough to have the transient time between them smaller than the intrinsic jitter of each single switch will report no advantage. The reason is that the pulse rise now will be dominated by the intrinsic jitter of the individual switches and not by the asymmetric switching.

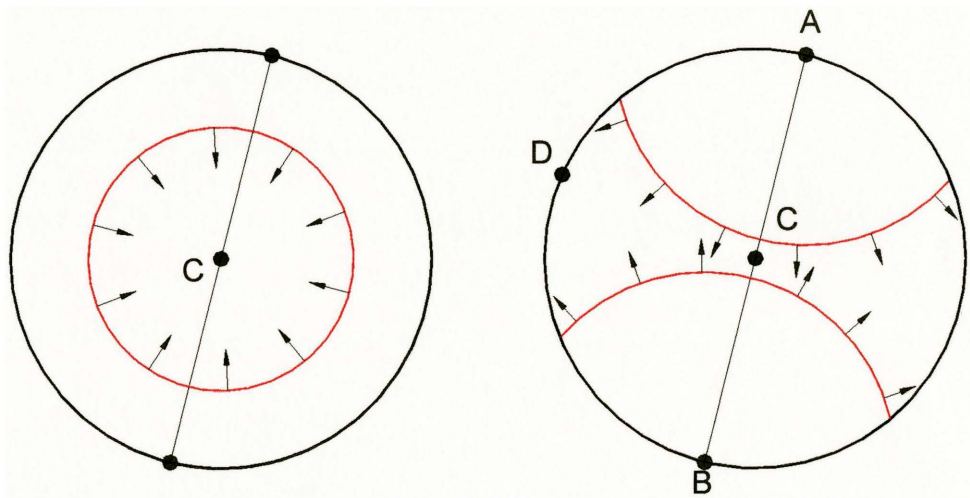

Figure 2.12. a) Front view of a circular Blumlein line switched by a continuos switch at the periphery that generates a symmetric wave towards C. b) Switching the Blumlein line at A and B generates an asymmetric wave.

To achieve switching in a distributed manner we utilized an array of seven spark-gap switches. Pressurized SF_6 trigatron switches are used to allow for command triggering with sufficient precision so that all seven parallel switches can close almost simultaneously (i.e. within the switch-to-switch transient time of about 1 ns). Figure 2.13

shows a cross sectional view of one of these switches and its assembly into the outer part of the Blumlein generator. This switch design resembles the generic trigatron type shown in fig. 2.6. The housing is made of poly-methyl-methacrylate (PMMA) with a 1 cm thick wall. The electrodes are made of brass and the entire arrangement is hold together by an aluminum cap that presses the entire switch against the middle plate of the Blumlein. The design is sufficiently strong to withstand a working pressure > 100 psi. The trigger signal is brought on a high voltage RG-213/U cable. The center conductor of this cable is inserted through the outer electrode and a solid stainless steel rod is used as the trigger pin. The outer braid of the cable is cut back several centimeters and clamped to the electrode to provide the trigger signal return path. The total inductance of a single switch is about 100 nH, and the total inductance for the entire array of less than 15 nH. A switching performance with a simultaneity of a few nanoseconds is inferred. The current has been observed to be shared approximately equally among the seven switches.

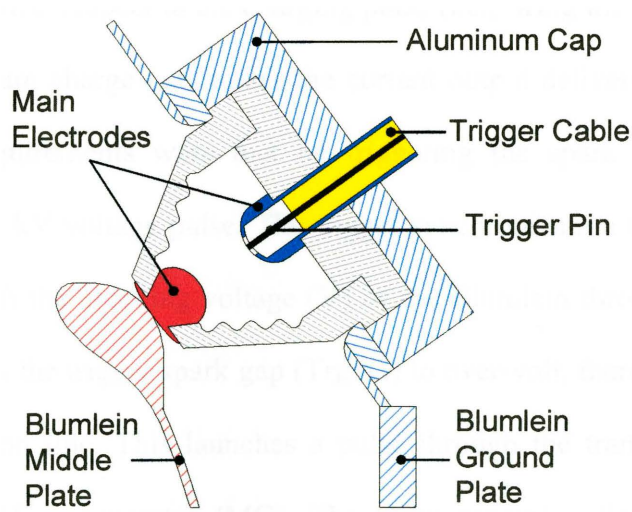

Figure 2.13. Schematic of the cross sectional view of one of the seven Blumlein line switches.

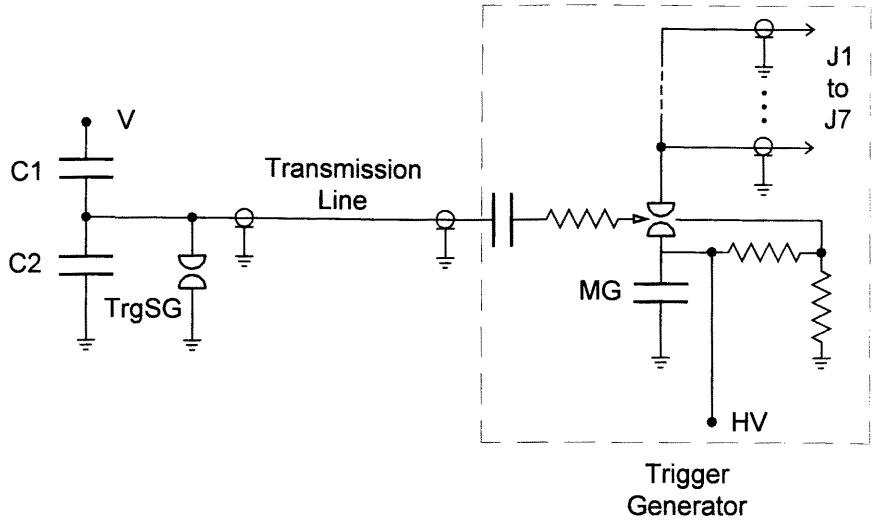

Figure 2.14. Trigger synchronization circuit. V = charging voltage, C1 and C2 = capacitive divider, TrgSG = spar-gap, MG = Mini-Marx generator, J1 to J7 = trigger outputs.

2.3. Trigger synchronization

As was mentioned before, to achieve a fast and clean current pulse it is very important to switch all the spark gaps in the Blumlein simultaneously. Another very important parameter for achieving an optimum performance is the time at which the Blumlein is switched with respect to the charging pulse (i.e., firing the Blumlein switches at the time of maximum charge maximizes the current output delivered to the capillary load). These two requirements were met by triggering the spark gap array with a self-synchronized 100 kV voltage pulse. The trigger synchronization circuit is shown in fig. 2.14. In this circuit the charging voltage (V) of the Blumlein through the capacitive divider (C1-C2) forces the trigger spark gap (TrgSG) to over-volt, thereby grounding one end of the transmission line. This launches a pulse through the transmission line that triggers a two-stage Marx generator (MG). The Marx generator discharges a 100 kV voltage pulse over a set of seven identical parallel transmission lines (J1 to J7 in fig. 2.14)

connected to the trigger pins of the Blumlein spark gaps, forcing the simultaneous switching of the spark gap array.

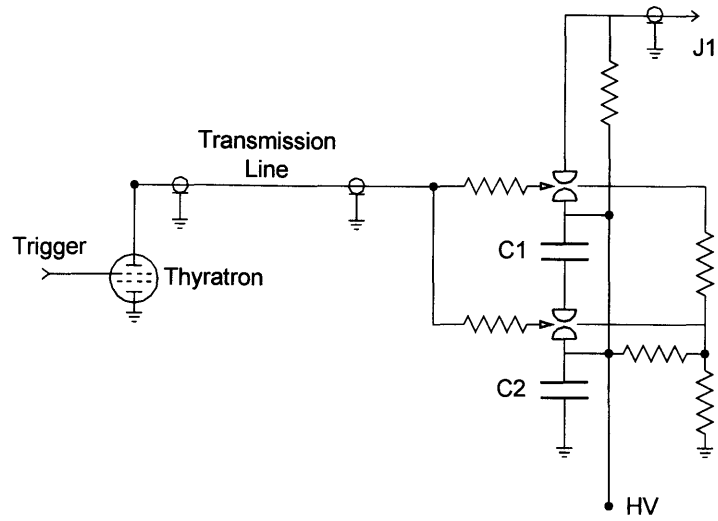

Figure 2.15. Pre-ionization generator circuit.

2.3.1. Pre-Ionization

In order to achieve gain in capillary discharge plasmas it is necessary to have a homogeneous and stable plasma column. These types of plasma columns are only obtained when the initial conditions of the plasma are uniform and well behaved. The best initial condition will be that of a one-dimensional homogeneous, partially or fully ionized plasma as is usually assumed in a magneto-hydro-dynamic (MHD) calculation. In order to obtain a homogenous pre-ionized plasma column a 10 kV pulse is applied 500 ms before the main current pulse across the capillary, achieving in this way a uniform break down. The current is limited to 1 mA so excessive pre-heating of the plasma is avoided. About 10 μs before the main current pulse a second pre-ionization current pulse is utilized to further ionize the plasma column (in this case a 100 A current is allow to flow through the capillary). Figure 2.15 shows the circuit of the pre-ionization

pulse generator. The generator circuit consists of a capacitor bank and a pressurized gas spark gap. The spark gap is triggered by a circuit similar at the one utilized to synchronized the Blumlein switches with the charging pulse, except that in this case the spark gap is replace by a hydrogen thyratron switch controlled by an external trigger signal.

2.4. Diagnostics

In the preceding sections of this chapter we have discussed the design and operation of the various components of the pulse generator. However without the proper means to measure the quantities produced by the system, one can hardly utilize them to generate the desired results. In this section we shall discuss the various measuring techniques and devices utilized to diagnose and operate the generator.

In high power systems, some of the most useful measured quantities are voltages and currents. Because the large magnitude and fast temporal behavior of these quantities, ordinary methods are no longer adequate to obtain accurate measurements and especial techniques must be applied.

A total of seven Rogowski coils, one capacitive voltage divider and a resistive voltage divider are employed throughout the experimental setup to monitor the operation of the different compression stages of the current pulse. Figure 2.16 shows the placement of the different devices associated with the capillary discharge. All the devices with, the exception of the Rogowski coil that measures the current through the capillary (RogCap), are utilized only for diagnostic and optimization proposes. The "Marx ground Rogowski" (RogMrx) is place in the Marx generator current return path to give information of the

amount of current delivered by the Marx Generator during the discharge period. A resistive voltage divider (ResWC) and a Rogowski coil (RogWC) are utilized to monitor the water capacitor charging voltage. The capacitive voltage divider (CapBln) is utilize to measure the charging voltage of the Blumlein while the Rogowski coil (RogBln) place in the Blumlein grounding inductor monitors the current to ground of the Blumlein. To monitor the current distribution though the Blumlein-switch array, three of the seven Blumlein switches are equipped with small Rogowski coils (RogSwt 1-2-3).

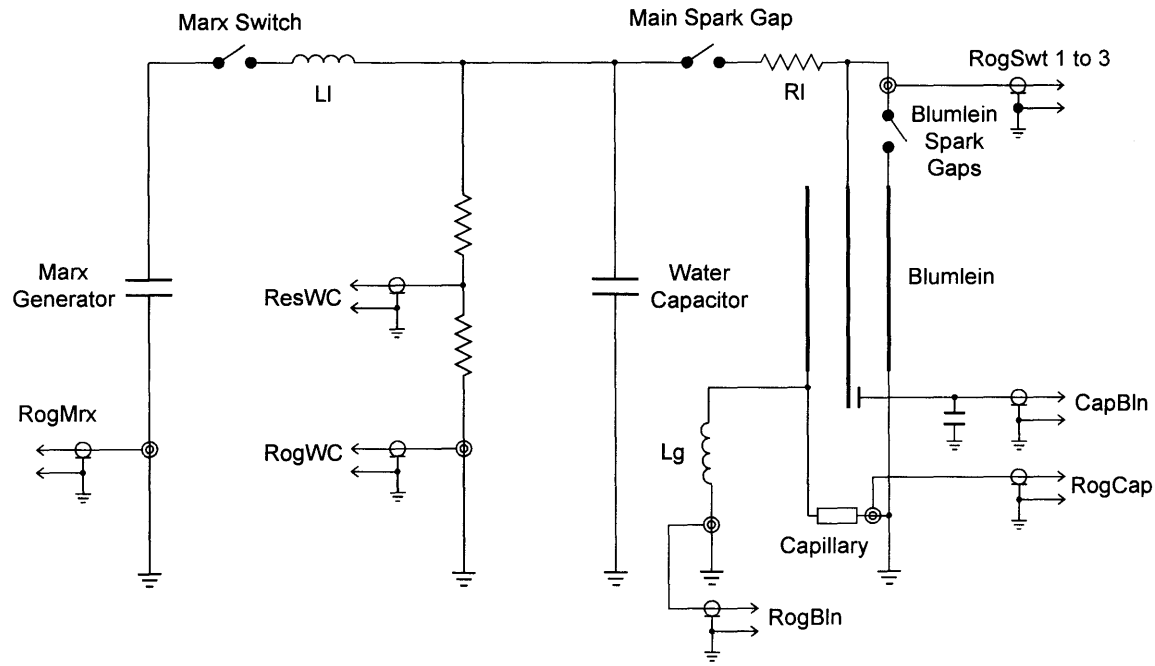

Figure 2.16. Equivalent circuit of the capillary discharge generator showing the emplacement of the different diagnostic devices.

2.4.1. Resistive Voltage Divider

An electrolytic resistive voltage divider is utilized to monitor the charging voltage of the water capacitor. The divider consists of a 5 cm diameter polyethylene tube filled with a copper sulfite solution. At both ends of the tube stainless steel electrodes

make electric contact with the solution. Figure 2.17 shows the actual design of the electrolytic divider in which the high voltage arm of the divider is define by the high voltage electrode and the low voltage electrode. If the stray capacitances are negligible, then the circuit can be represented by that shown in fig 2.17. From this figure, one can see that the divider works as a single-pole low-pass filter with a cut-off frequency of (R1 + R2) / Lg and a DC attenuation of R2 / (R1 + R2), for this reason it is essential to make the circuit inductance Lg as low as possible. This is one of the reasons why the high voltage divider is constructed with a liquid dielectric (R1, R2). The basic rule for designing a resistive voltage divider is that the value Lg / (R1 + R2) < tr / 20, where tr is the rise time of the voltage to be measured. The low voltage arm resistance (R2 = 50 Ω) is matched so reflection problems between the divider and the coaxial cable used to connect the divider to the input end of the scope are avoided.

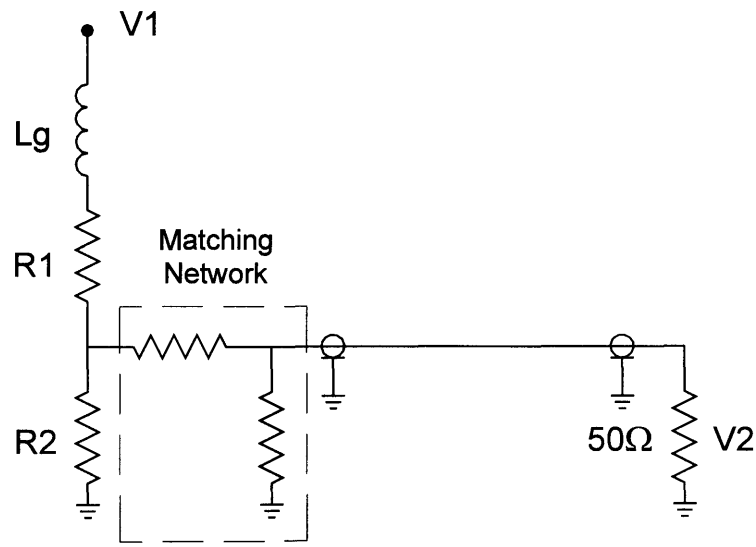

Figure 2.17. Equivalent circuit of a resistive voltage divider, R1 and R2 actual resistive divider, Lg = circuit inductance.

2.4.2. Capacitive Voltage Divider

The charging voltage of the Blumlein can be monitored by means of a capacitive voltage divider. The reason to employ a capacitive voltage divider over a resistive divider is its better temporal response. However, the capacitive divider has the disadvantage of been susceptible to the effect of undesirable oscillations in the output voltage, when there is same inductance in the circuit [2.1]. One way to lessen the effect is to employ capacitors having low inductance. The basic structure of the capacitive voltage divider is quite similar to that of a resistive voltage divider except that in this case the resistors are replaced with suitable capacitors. Figure 2.18a show the circuit of the capacitive divider employed in this experiment. C1 and C2 represent the high voltage and low voltage arms of the divider respectively. R1 and R2 define a matching network utilized to match the impedance of the divider to the 50 Ω impedance of the coaxial cable and the oscilloscope. The entire circuit behaves like a single-pole, single-zero, high-pass filter with a droop time of tr = (C1 + C2)(R1 + R2). This time is chosen to be 6 μs, which is large enough for our application. The actual structure of the capacitive divider is show in figure 2.18b, where C2 is a high voltage ceramic capacitor and R1 and R2 are thin film low inductance resistors.

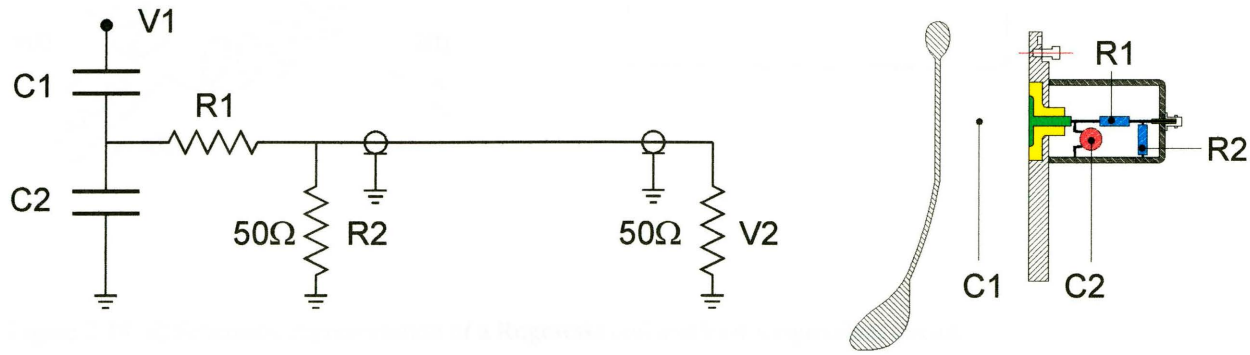

Figure 2.18. a) Capacitive voltage divider and b) basic structure of the capacitive voltage divider.

2.4.3. Rogowski Coil

The Rogowski coil is a type of field-coupled sensor that utilizes the induce voltage in the secondary coil to determine the primary current. Figure 2.19a shows the basic structure of a Rogowski coil, it consist of N small loops forming a nearly complete circle. The primary current to be determined is complete encircle by the secondary coil. This is equivalent to having a primary coil of one turn. Depending on the design and the application, the Rogowski coil can be used to either measure the magnitude and pulse form, or the time rate of change of the primary current [2.2]. The equivalent circuit of the secondary is shown in figure 2.19b. If the characteristic time tc of the signal is such that $tc << L / (Z + R)$ then the voltage V across the resistance Z is proportional to the primary current I, $V = I Z / N$. Shielding the coil from external interference is an important issue, however a proper slit opening must be left in the shield, in order to allow the magnetic field to penetrate into the coil.

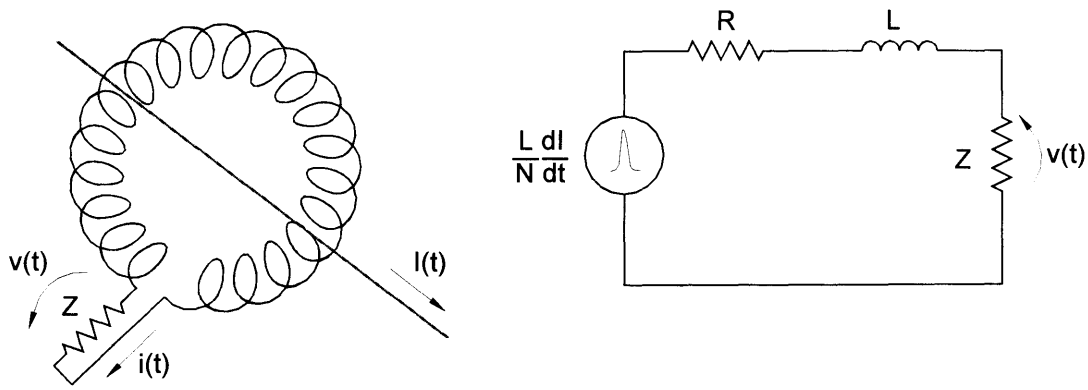

Figure 2.19. a) Schematic representation of a Rogowski coil and b) it's equivalent circuit.

2.5. References

2.1. N. W. Harris, "Measurement of Electrical Quantities in pulsed Power Systems", Ed. By R. H. Mcknight and R. E. Hebner, *NBS special publication* **628**, pp. 20, USA 1982.

2.2. G. Sower, *3rd IEEE Pulse Power Conf.*, pp. 189, 1981.

CHAPTER 3

PLASMA COLUMN CHARACTERIZATION

3.1. Introduction

This chapter discusses the results of the study of capillary discharge plasma columns created using the pulse generator discussed in chapter 2. The objective of these measurements was to obtain information on the plasma parameters, and geometrical characteristics of capillary plasmas created under the significantly greater excitation power allowed by the new high power generator. Of particular interest are the degree of ionization, electron temperature, plasma density, and final column diameter. Knowledge of these parameters is required to demonstrate the capability of extending discharge-pumped lasers to significantly shorter wavelengths [3.1]. In addition, the measurements also provide some information on the important issue of the reproducibility and uniformity of the plasma column, that are major requirements for effective soft x-ray amplification [3.2].

Argon was selected as a test gas to conduct the first series of studies with this new high power pulse generator. While argon is not a candidate for lasing at wavelengths shorter than 46.9 nm, it was selected because its well known extreme-ultraviolet (XUV) [3.3] spectra allows a convenient test of the plasma conditions that can be achieved with increased excitation.

3.2. Polyacetal Capillaries

In this section we describe results obtain using time-resolved pinhole images and time-resolved extreme-ultraviolet spectroscopy of plasma columns generated in polyacetal $(CH_2O)_n$ capillaries. The measurements were conducted in 4 mm in diameter, 1 cm long capillaries.

3.2.1. Time resolve pinhole images

The radial evolution of the plasma columns generated in 4 mm diameter capillaries was studied by means of an on-axis pinhole camera. The experimental setup used for these measurements is schematically illustrated in figure 3.1. A 90 μm pinhole was utilized to image the plasma onto the detection plane with a magnification of 3.5x and a spatial resolution of 60 μm. The gated detection system consisting of a Multi-Channel-Plate (MCP) intensified Charge-Coupled Device (CCD) array detector which had a time resolution of ≈ 4 ns. Wavelength discrimination was obtained using a 1 μm thick carbon filter, or a stack composed of a 1 μm carbon filter and one or two 0.1 μm aluminum filters respectively. This technique permits discrimination between the hot emitting regions and the cold emitting regions of a plasma column. The transmission

efficiencies corresponding to each of these three filter configurations are plotted in figure 3.2 [3.4]. The carbon filter alone transmits photons with wavelength between 45 to 100 Å and also below 20 Å. The addition of a 0.1 μm thick aluminum filter decreases the transmisivity in the region between 4.5 to 10 nm by a factor ≈ 5. The addition of an extra 0.1 μm thick aluminum filter reduces the transmisivity in this region by a factor ≈ 15 with respect to the carbon filter alone, practically limiting the transmitted radiation to wavelengths below 20 Å.

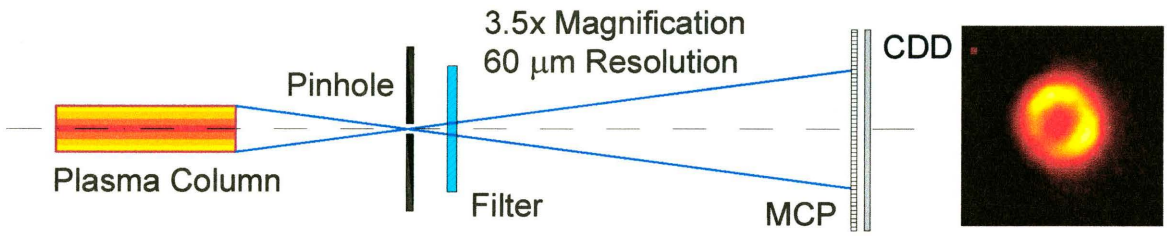

Figure 3.1. Schematic representation of the experimental set up used to obtain time-resolved pinhole images of the capillary plasma.

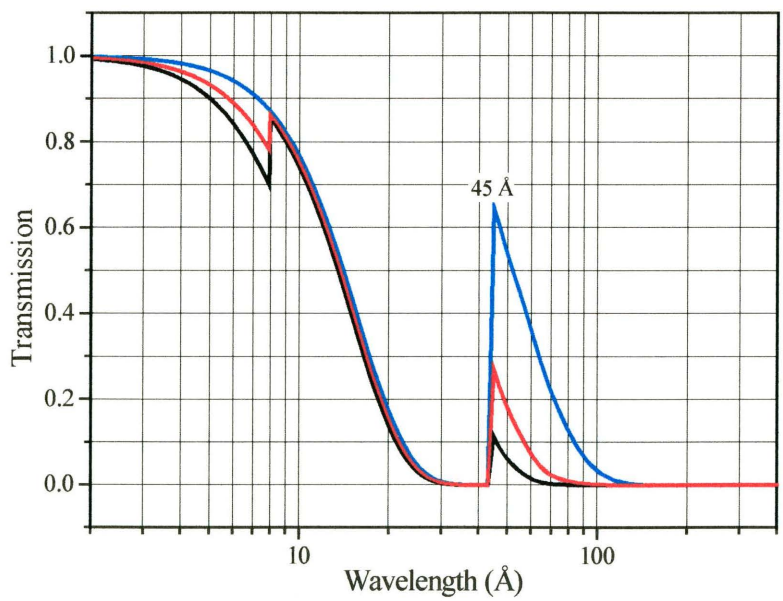

Figure 3.2. Transmission characteristics of a 1 μm thick carbon film (blue line), 1 μm of carbon plus 0.1μm of aluminum (red line) and 1μm of carbon plus 0.2 μm of aluminum (black line) [3.4].

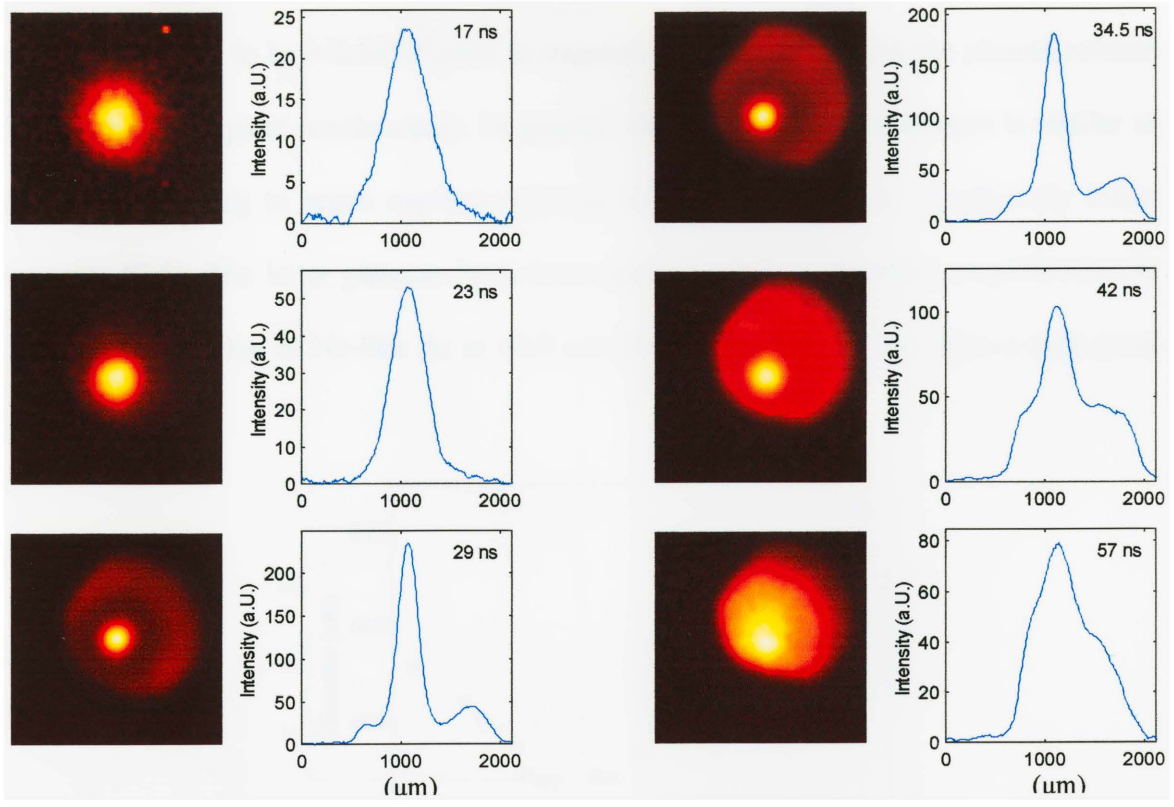

Figure 3.3. Series of time resolve on-axis pinhole images of a polyacetal capillary plasma column filtered with a 1 μm thick carbon film. Time with respect to the initiation of the current pulse is indicated in each image. A horizontal cross section of the intensity distribution is shown with each image. The color intensity in each image was normalized. The non-symmetric features observed at large diameters are due to the fact that the plasma column is not centered respect to the differential pumping pinhole, which cuts part of the image.

Figure 3.3 show a sequence of time resolve pinhole images depicting the evolution of argon plasma columns filtered with a 1 μm thick carbon filter. They correspond to plasmas generated by a 183 kA current pulse with a 10-90 % rise time of 13 ns through a 4 mm diameter, 1 cm long polyacetal capillary filled with 1.3 Torr of argon. The corresponding evolution of the FWHM diameter of the soft x-ray emitting region of the plasma relative to the beginning of the current pulse is show in figure 3.4. The fast current pulse detaches the plasma from the walls, compressing the plasma column to its final diameter. From figure 3.4 the collapse of the plasma column to a minimum FWHM of ≈ 250 μm is observe to happen $\cong$ 29 ns after the initiation of the current pulse. The radial velocity of the region at the wavelengths selected by the carbon

filter is observed to be $\approx 2.6 \times 10^6$ cm/s at stagnation. After stagnation the plasma column is observed to expand continuously. In general, the symmetry of the images is similar to that corresponding to argon capillary plasma columns generated at significantly lower currents [3.5]. The latter plasmas have been used to produce saturated amplification in the 3p-3s J = 1 line of Ne-like Ar at 46.9 nm [3.6] and are known to have a very good axial uniformity.

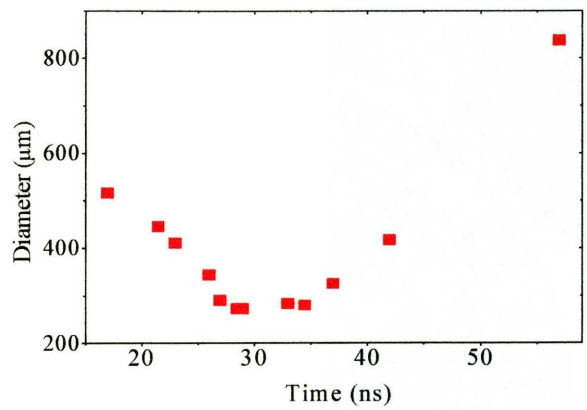

Figure 3.4. Measured diameter of the plasma column as a function of time as observed utilizing a 1 μm thick carbon filter. The data corresponds to a 4 mm in diameter polyacetal capillary with an initial argon pressure of 1.3 Torr. The peak discharge current was of 183±5 kA with a 10-90 % rise time of 13 ns.

Figure 3.5 shows the time evolution of a plasma column filtered by a 1 μm thick carbon filter and a 0.1 μm thick aluminum filter. The discharge conditions for this sequence are the same as those in figure 3.3 but, they utilize current pulses of ≅ 184 kA with a 10-90 % rise time of ≅ 12 ns. This sequence shows qualitatively the same behavior observed with the 1 μm carbon filter. A pinch diameter of ≅ 290 μm in is observed ≅ 25 ns after the initiation of the current pulse. The difference in the pinch time between the two sequences is possibly due to the differences in the current pulses. Measurements utilizing two aluminum filters plus a carbon filter did not reveal any additional information.

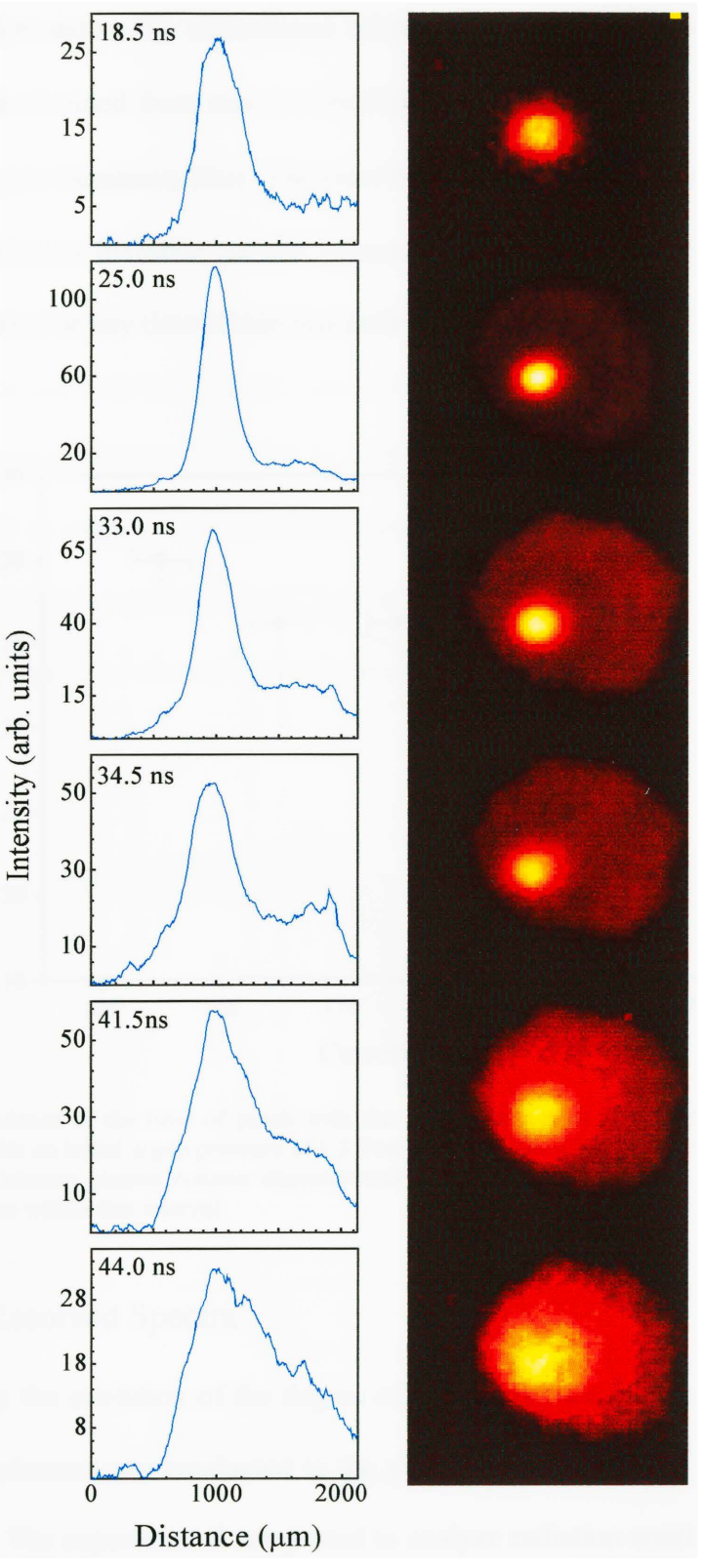

Figure 3.5. Sequence of time-resolved pinhole images filtered by a 1 μm thick carbon film plus a 0.1 μm thick aluminum film. The initial conditions are those of figure 3.3 but with an excitation current pulse of 185 kA and a 10-90 % rise time of 12 ns.

Figure 3.6 shows the dependence of the pinch time on the excitation current. These data were obtained from time-resolved pinhole images filtered by a 1 μm carbon filter plus a 0.1 μm aluminum filter. The error bars indicate the time interval between the image with minimum diameter plasma column and the previous image, as the actual pinch may occurred at any time within this interval.

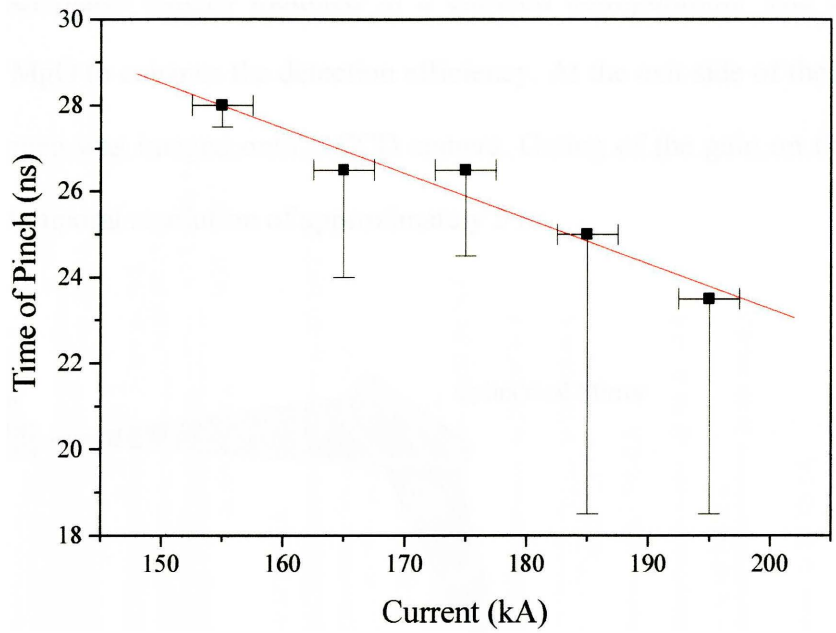

Figure 3.6. Dependence of the time of pinch with the excitation current for 4 mm diameter polyacetal capillaries filled with an initial argon pressure of 1.3 Torr. The error bars indicate the time interval between the image with minimum plasma column diameter and the previous image, since the actual pinch may occurred at any time within this interval.

3.2.2. Time Resolved Spectra

To study the evolution of the degree of ionization time-resolved spectroscopy of these capillary plasmas was conducted in the spectral region covering the range between 3 nm to 30 nm. The experimental setup used to analyze radiation emitted by the capillary discharge is shown in figure 3.7. The radiation from the plasma was collected and

focused through the slit of a 1 m grazing incidence spectrometer by a cylindrical gold-coated mirror placed at a grazing angle of 2° with respect to the incoming radiation. A fast shutter was used to protect the optical elements of the spectrometer against particles arising from the electrodes and capillary walls.

The spectrometer contains a gold-coated grating ruled at 1200 line per millimeter, placed at 4° gracing incidence angle. An intensified array detector consisting of two micro-channel plates (MCP) mounted in a chevron configuration. The front plate is coated with MgO to enhance the detection efficiency. At the exit side of the MCPs, a P20 phosphor screen was imaged onto a CCD camera. Gating of the gain on the front MCP allowed for temporal resolution of approximately 5 ns.

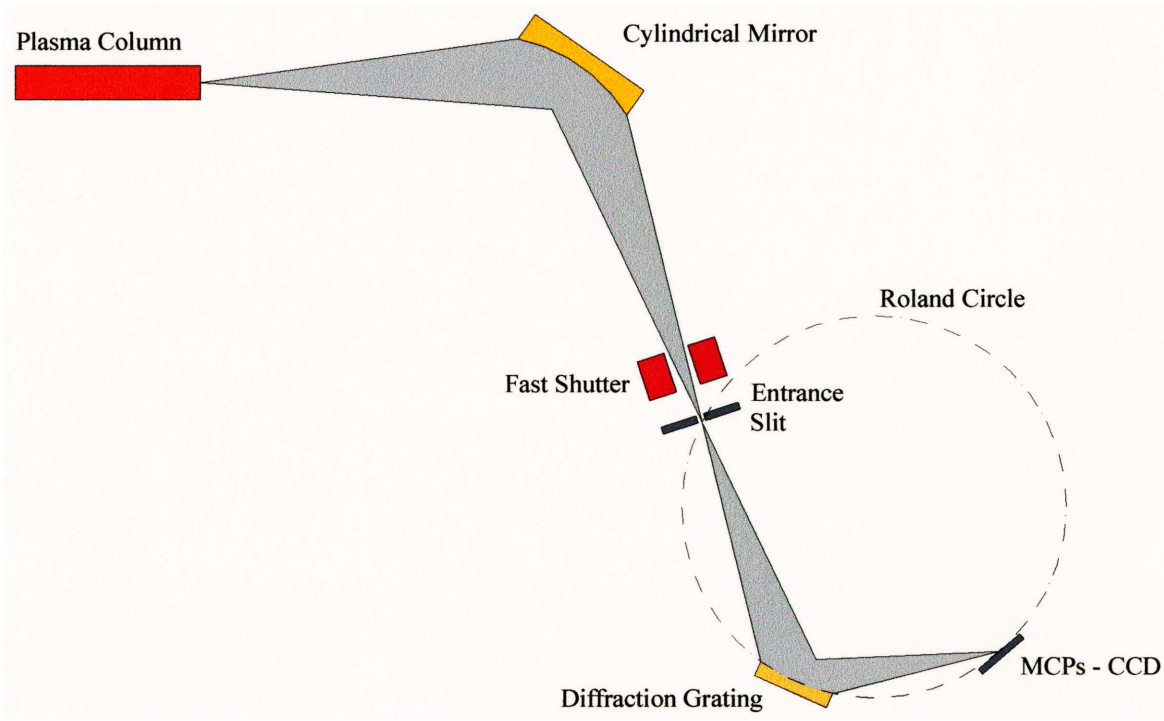

Figure 3.7. Experimental setup used to analyze the laser radiation emitted by the capillary discharge.

The spectral range between 18 nm to 23 nm was found to be suitable to study the time evolution of the ionization degree of the plasma, as it contains spectral lines belonging to all the ionization stages between ArXI through ArXV. An argon spectrum corresponding to the time of maximum ionization for a 197 kA current pulse and a 10-90 % rise time of about 11 ns is shown in figure 3.8. Argon lines corresponding to all ions with charge ranging from ArXI to ArXV are present. Strong line emission from ArXIV and ArXV is observed.

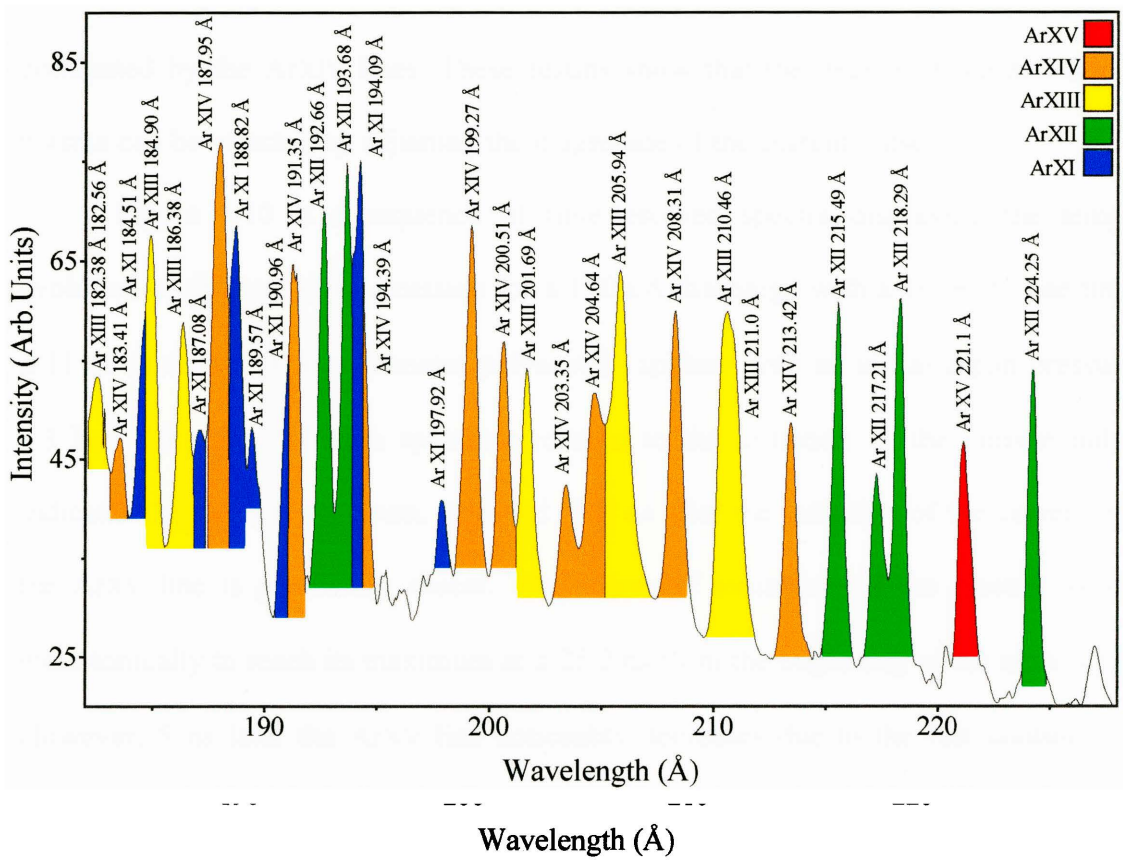

Figure 3.8. Line identification for an Argon spectrum corresponding to the time of maximum ionization in a polyacetal capillary 4 mm in diameter. The discharge current was 197 kA with a 10-90 % rise time of ≅ 11 ns and the initial argon pressure was of 1.3 Torr.

The relative intensity of the lines originating from the different charge states was used to monitor the degree of ionization as a function of current. Figure 3.9 shows time-resolved spectra of the soft x-ray emission from argon plasmas generated in 4 mm diameter, 1 cm long polyacetal capillaries for four different current pulses of increasing current. For the 150 kA discharge the most intense lines in the spectral region correspond to ArXII and ArXI, but ArXIV lines are also observe. As the current increases, the plasma becomes more highly ionized, as shown by the increase in the intensity of the ArXIV lines and by the relative decrease of the ArXI lines. At 180 kA the ArXV line begins to be noticeable. Finally at 190 kA the ArXV is clearly distinguishable and the spectrum is dominated by the ArXIV lines. These results show that the degree of ionization of the plasma can be selected by adjusting the magnitude of the current pulse.

Figure 3.10 is a sequence of time-resolved spectra displaying the temporal evolution of the soft x-ray emission for a 190 kA discharge with a 10-90 % rise time of $\cong$ 11 ns thought a 4 mm diameter polyacetal capillary with an initial argon pressure of 1.3 Torr. The time of each spectrum relative to the initiation of the current pulse is indicated. In the first spectrum, obtained 22.8 ns after the initiation of the current pulse, the ArXV line is practically absent. The degree of ionization of the plasma increases monotonically to reach its maximum at $\cong$ 25.2 ns from the beginning of the current pulse. However, 5 ns later the ArXV line noticeably decreases due to the fast cooling of the plasma after stagnation. This time of maximum ionization agrees with the time at which we observe the maximum compression of the plasma column (see fig. 3.4).

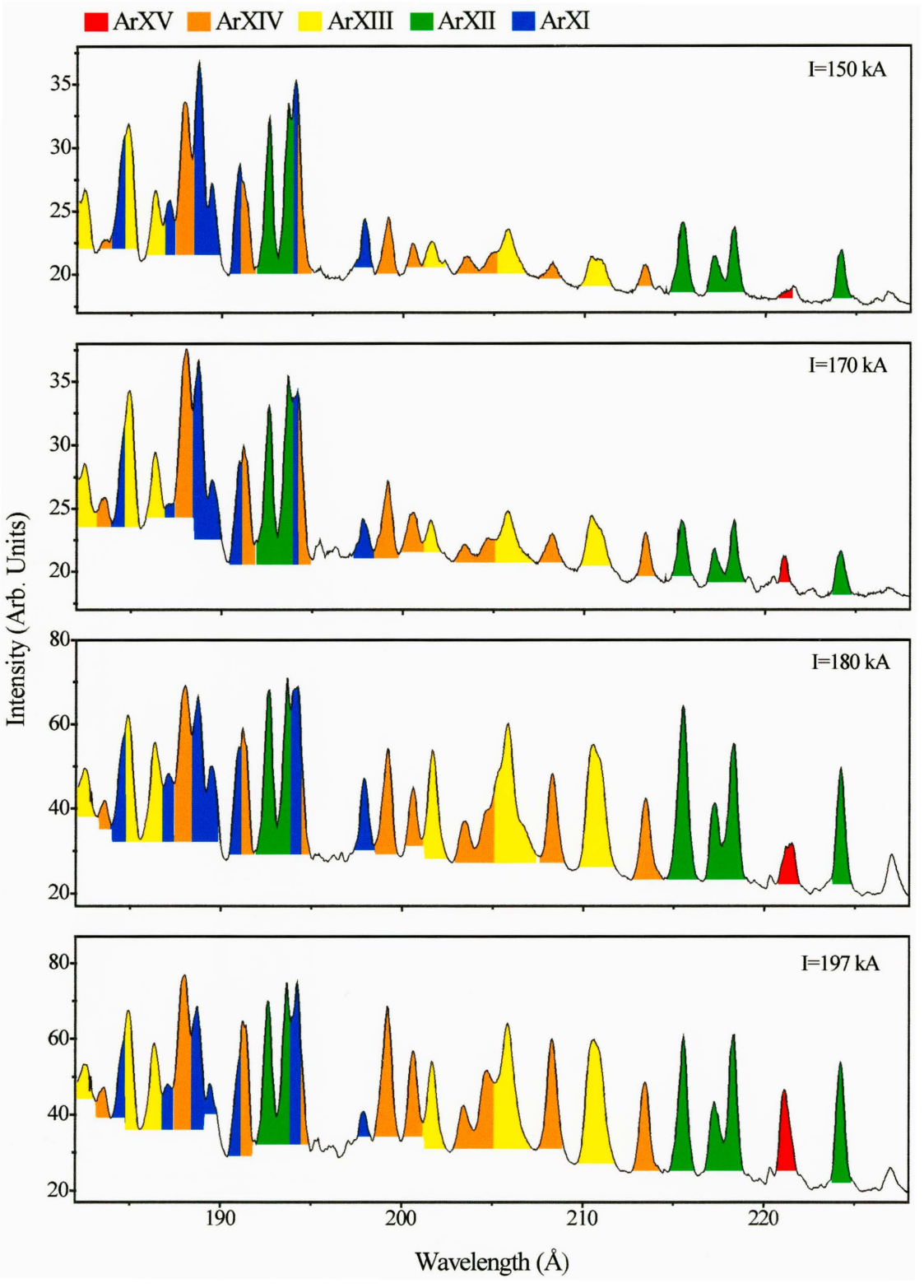

Figure 3.9. Dependence of the degree of ionization with the excitation current in 4 mm diameter polyacetal capillaries filled with 1.3 Torr of argon.

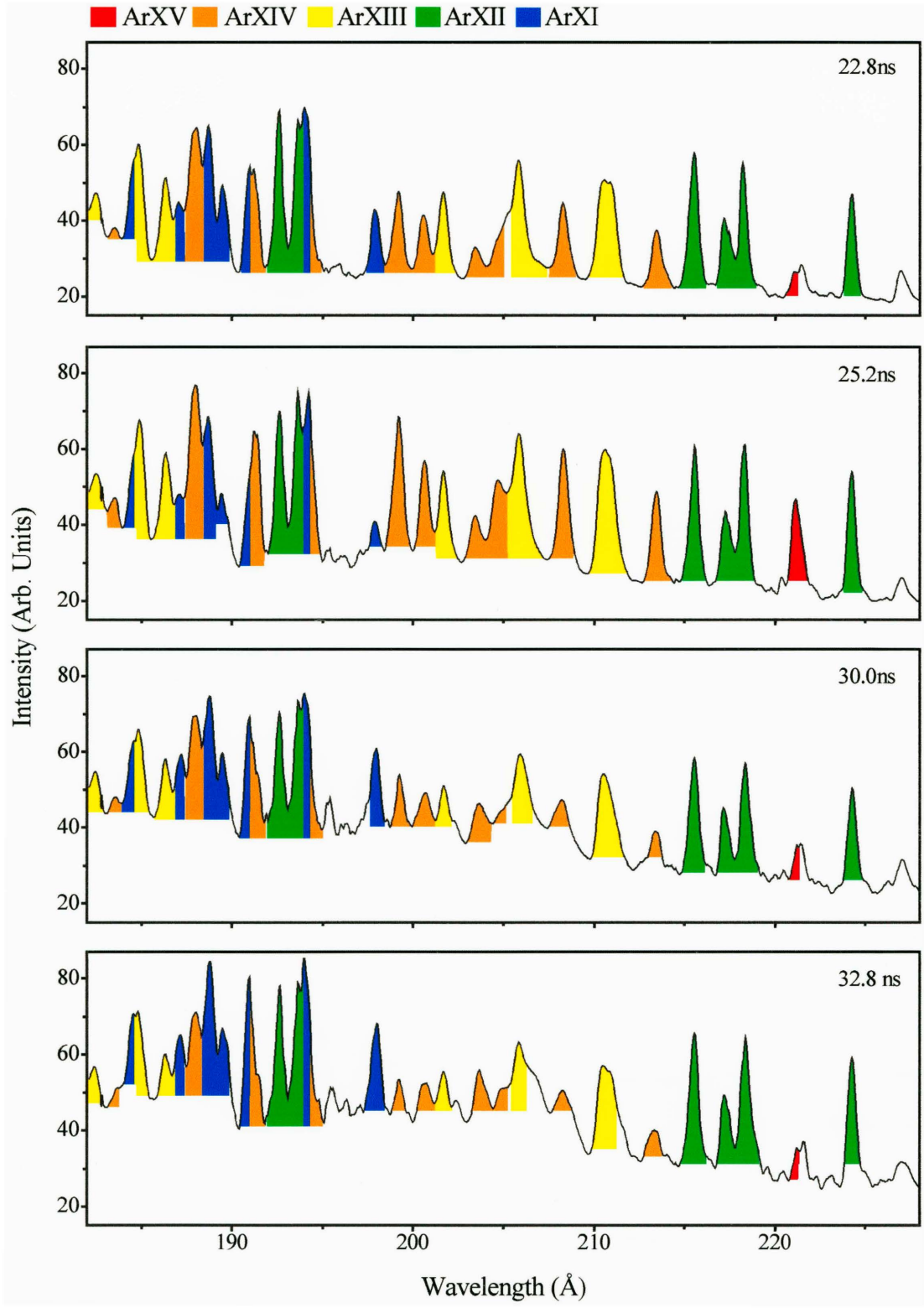

Figure 3.10. Sequence of spectra illustrating the time evolution of the degree of ionization for polyacetal capillary 4 mm in diameter for excitation currents of 195 kA and a 10-90 % rise time of ≅ 11 ns.

We have compared these measurements with the results of atomic/hydrodynamic model computed using the code RADEX [3.7]. Calculations of the degree of ionization and plasma dimensions are in general agreement with the data. Figure 3.11 show the computed radial profile of the electron temperature and density at the time of maximum ionization for a 197 kA discharge through a 4 mm diameter, polyacetal capillary filled with an initial argon pressure of 1.3 Torr. The temperature and density on axis are predicted to be 275 eV and 1.3×10^{20} cm^{-3}. Synthesized XUV spectra corresponding to these conditions showed general features that are in good agreement with the measured spectra. The compressed plasma diameter is computed to be 250-300 μm at ≅ 25 ns after the initiation of the current pulse; also this is also in agreement with the size of the soft x-ray-emitting region observed at the time of maximum compression.

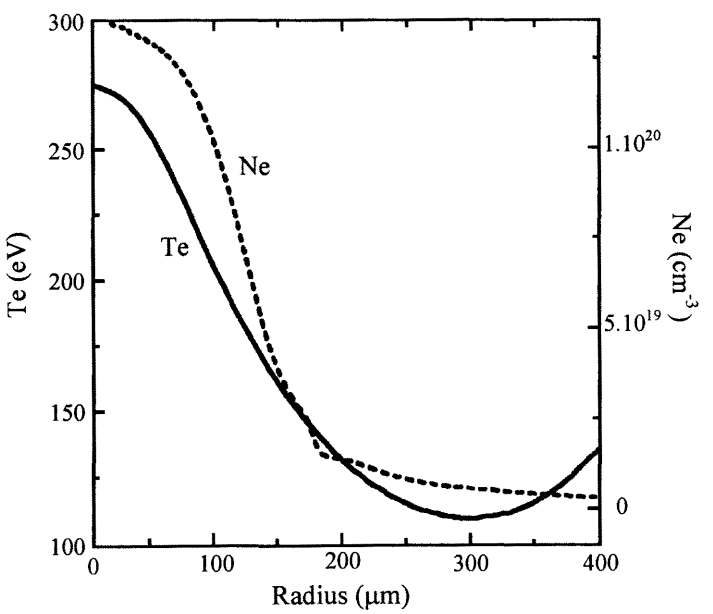

Figure 3.11. Computed electron temperature and density profiles of an argon filled 4 mm polyacetal capillary at 1.3 Torr and 197 kA with a 10-90 % rise time of ≅ 11 ns at the time of maximum ionization [3.7].

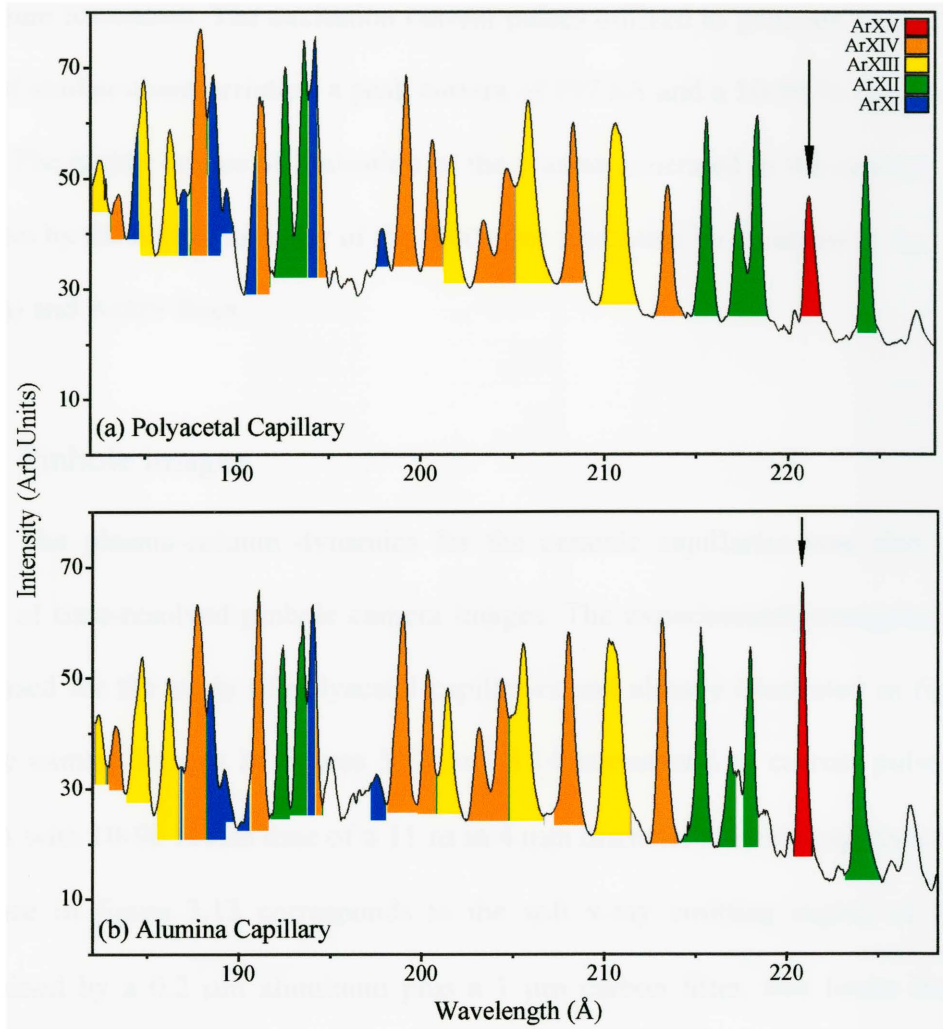

Figure 3.12. Time resolve spectra corresponding to polyacetal (a) and alumina (b) capillaries at the time of maximum ionization. The arrow is pointing to the ArXV line utilized as an indicator of the degree of ionization of the plasma column. The peak current was of 197 kA with a 10-90 % rise time of about 11 ns.

3.3. Ceramic Capillaries

To reduce the effects of wall ablation with the goal of obtaining hotter plasma columns, alumina capillaries were tested. The results showed that capillary plasmas with a significantly higher degree of ionization are obtain when ceramic capillaries are utilized in comparison with polyacetal capillaries. As an example, figure 3.12 shows two typical spectra corresponding to the 18-23 nm spectral region for ceramic and polyacetal capillaries of the same diameter (4 mm). Both spectra were obtained near the time of

maximum ionization. The excitation current pulses utilized to generate these two spectra were of similar characteristics: a peak current of 197 kA and a 10-90 % rise time of about 11 ns. The higher degree of ionization of the plasma generated in the ceramic capillaries is shown by the higher intensity of the ArXV line (indicated by an arrow at the right of the spectra) and ArXIV lines.

3.3.1. Pinhole images

The plasma-column dynamics for the ceramic capillaries was also studied by means of time-resolved pinhole camera images. The experimental arrangement was the same used for the study of polyacetal capillaries and already illustrated in fig. 3.1. The pinhole camera images in figures 3.13 and 3.14 correspond to current pulses of about 190 kA with 10-90 % rise time of ≅ 11 ns in 4 mm diameter alumina capillaries. The time sequence in figure 3.13 corresponds to the soft x-ray emitting region of the plasma determined by a 0.2 μm aluminum plus a 1 μm carbon filter, that limits the radiation detected mostly to wavelengths below 20 nm. This sequence of images shows the formation of a plasma sheath that evolves to form a compressed plasma column at the center of the capillary. The earliest image, obtained at 20 ns from the beginning of the current pulse, shows a cylindrical shell with an outer diameter of ≅ 815 μm caused by the current distribution that is influenced by the skin effect. The subsequent images show the rapid continuos compression of the plasma column. The soft x-ray-emitting region of the plasma reaches its minimum diameter of ≅ 250 μm at about 25 ns after the beginning of the current pulse after reaching a radial velocity of ≅ 0.7×10^7 cm/s. This result is in good agreement with the predictions of hydrodynamic computations, which predict that the

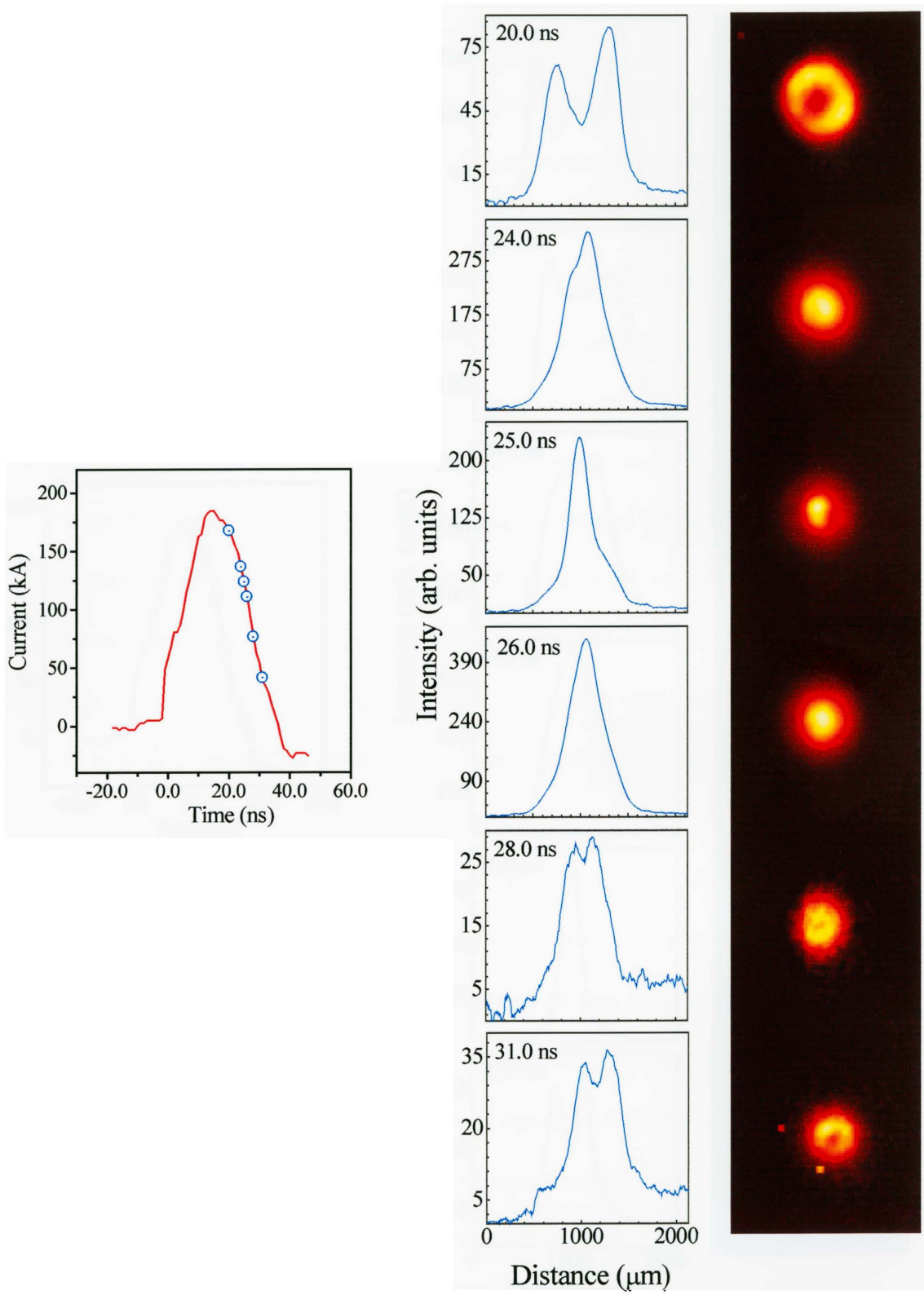

Figure 3.13. Time resolve pinhole camera images for a 4 mm in diameter ceramic capillary taken utilizing a 1 μm thick carbon filter plus 0.2 μm thick aluminum filter and a current pulse of 190 kA with a 10-90 % rise time of ≅ 11 ns.

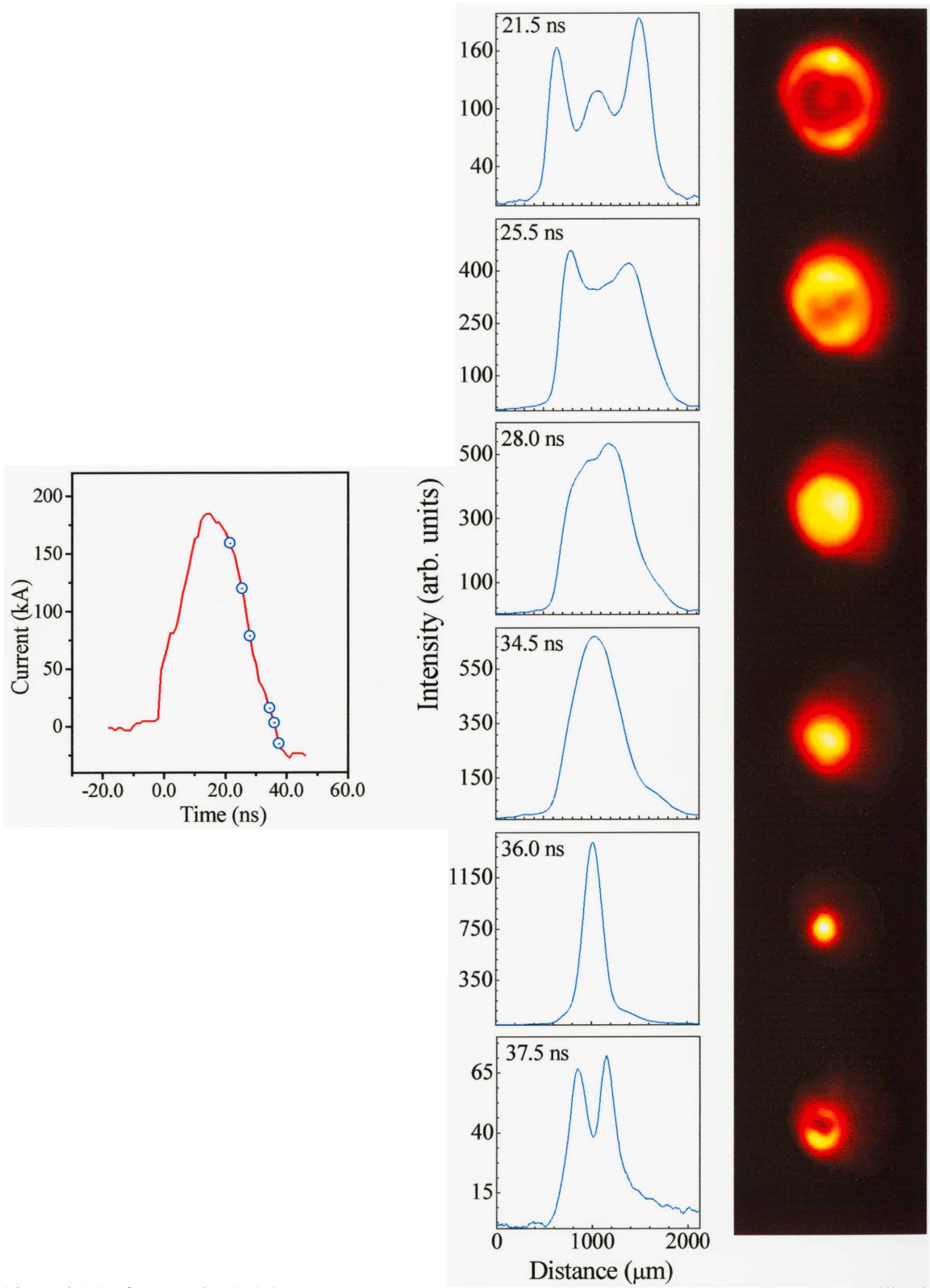

Figure 3.14. Time-resolved pinhole camera images for a 4 mm in diameter ceramic capillary taken utilizing a 1 μm thick carbon filter and an excitation current pulse of 190 kA with a 10-90 % rise time of ≅ 11 ns.

plasma column collapses near this time. Subsequently the plasma column expands and the intensity of the radiation emitted within this spectral range decreases by nearly an order of magnitude in the next 3 ns. For times later than 31 ns the intensity drops below the detection limit. It should be noticed that the asymmetry observed in the wings of the profiles corresponding to the larger diameter images is caused by an imperfect alignment of the pinhole rather than by an asymmetry in the plasma column. These results show a similar behavior at the one observed in the polyacetal capillaries.

Figure 3.14 shows a series of pinhole images obtained with only a 1 μm carbon filter. The removal of the aluminum filter adds to the detected wavelengths the spectral region between 40 nm to 100 nm (see fig. 3.2). The formation and collapse of a plasma sheath is also clearly observed in this sequence, but in this case the pinch observed in figure 3.13 is largely masked by photons with longer wavelengths, that at this time of the compression are emitted over a much broader region. However, figure 3.14 clearly shows the occurrence of a latter pinch that takes place at $\cong$ 36 ns from the beginning of the current pulse. This second pinch was not observed with the stack of the two filters, which only monitors wavelengths below 2 nm. This suggests that it corresponds to a colder plasma. The difference between the evolution of the soft x-ray emitting region observed with and without the aluminum filter is shown in figure 3.15. This second pinch was not observed in the pinhole sequences made with polyacetal capillaries. The apparent absence of the second pinch might be explained by the significantly larger amount of ablated material that gives the second pinch significantly lower temperature and larger diameter, and therefore makes it more difficult to detect.

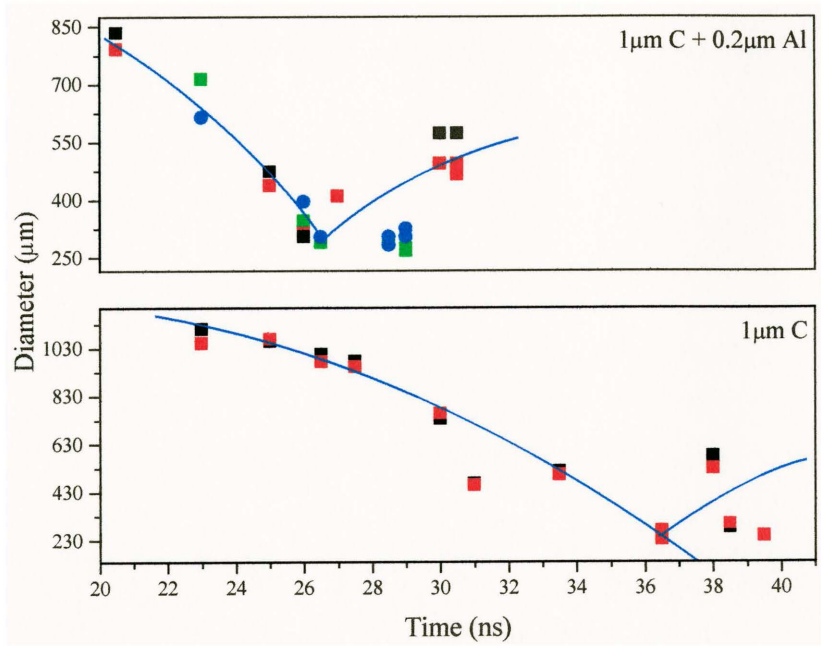

Figure 3.15. Comparison of the evolution of the plasma diameter as observed through a 1 μm thick carbon filter plus a 0.2 μm thick aluminum filter and only a 1 μm thick carbon filter.

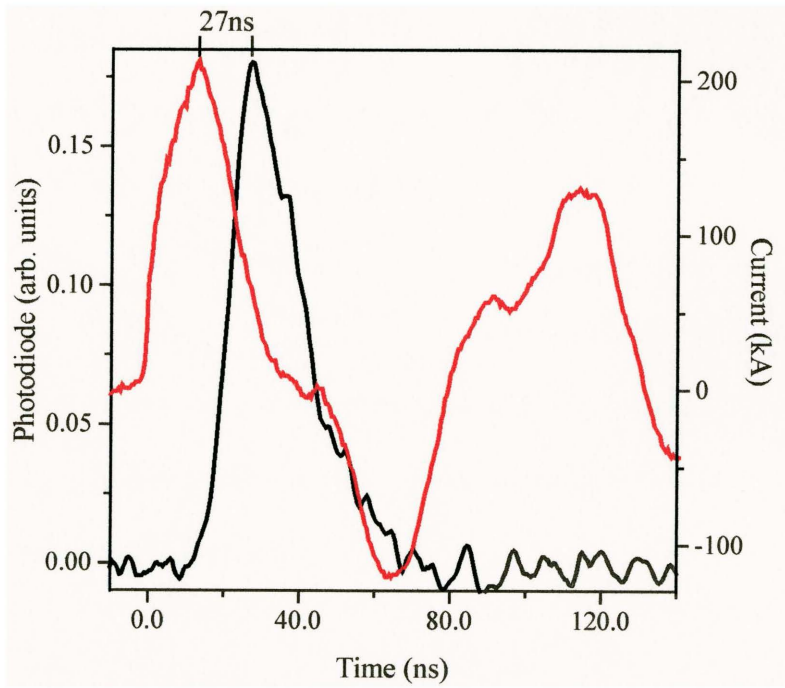

Figure 3.16. Correspondence of the signal obtained utilizing a fast MCP intensified vacuum photodiode filtered by a 1 μm thick carbon film plus a 0.2 μm thick aluminum film (black trace) with the excitation current (red trace) through a 4 mm in diameter ceramic capillary.

Figure 3.16 shows the correspondence of the signal obtained utilizing a fast MCP intensified photodiode filtered by a 1 μm thick carbon film plus a 0.2 μm thick aluminum film with the excitation current through a 4 mm in diameter ceramic capillary. The 212 kA current pulse starts 27 ns before the emission peak detected by the photodiode.

3.3.2. Spectra of Plasmas Generated in Ceramic Capillaries.

The series of time resolved spectra in figure 3.17 and 3.18 provide information of the temporal variation of the degree of ionization of the plasma for discharges in ceramic capillaries with 3 mm and 4 mm diameters, respectively. The peak amplitude and the 10-90 % rise time of the current pulses were maintained approximately constant for these two series at 190±5 kA and 11.5±1.5 ns respectively. The relative intensity of the ArXV line and the changing ratio of intensities between the two adjacent lines of ArXIV and ArXI at 18.8 nm and 18.9 nm respectively give an indication of the variation of the degree of ionization. The maximum ionization is observed to occur around the time corresponding to the first pinch, in the vicinity of 25 ns. Figure 3.17 shows that the ArXV line is almost absent at 19.6 ns after the beginning current pulse but is dominating only 2 ns later. Although the time of pinch is similar for ceramic and polyacetal capillaries the degree of ionization achieved in the ceramic capillaries is considerably larger than the one obtain in the polyacetal capillaries. This is easy to tell from the relative intensities of the Ar XV line in figures 3.10 and 3.18.

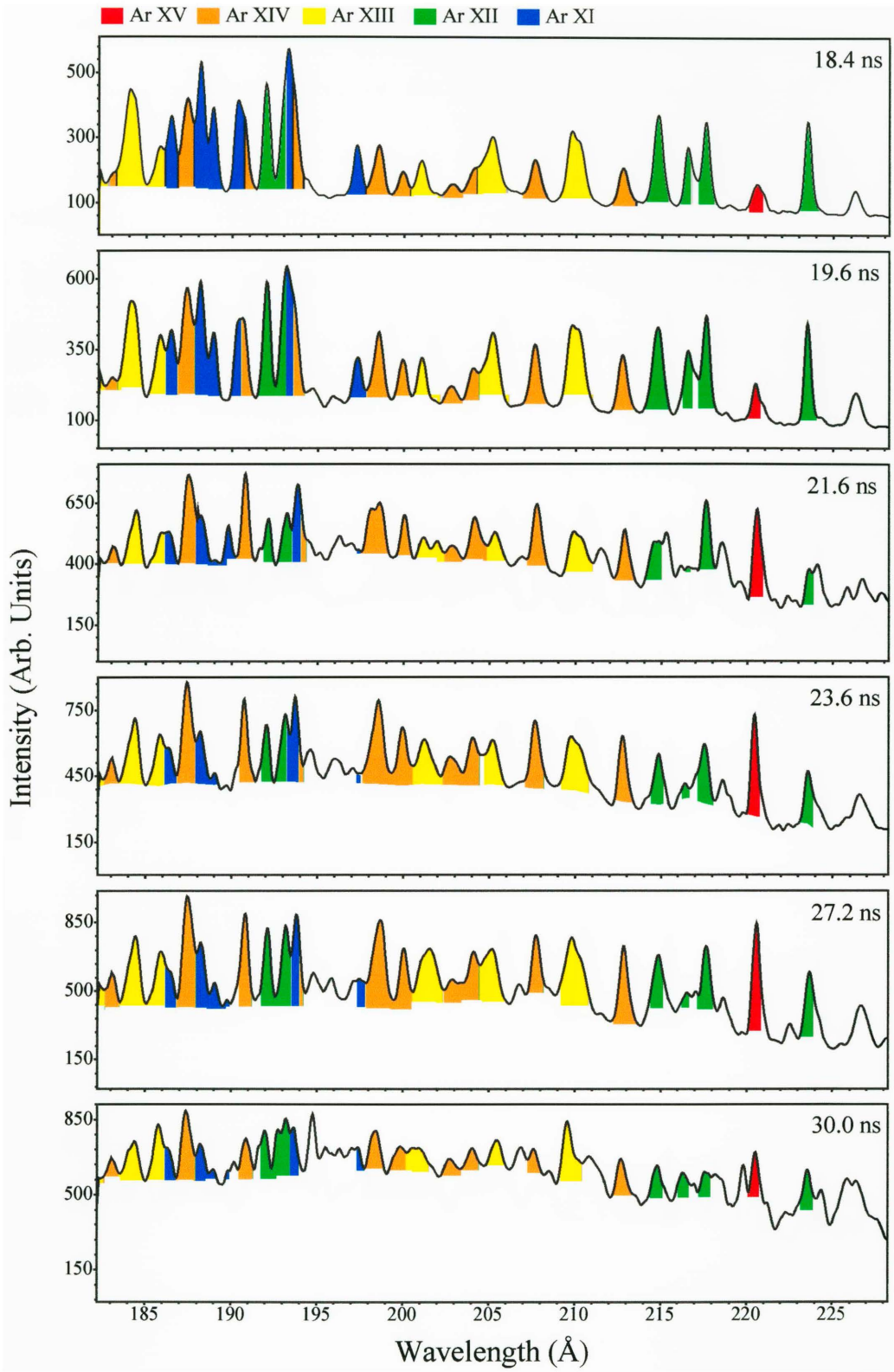

Figure 3.17. Time evolution of spectra that reveal the degree of ionization in a 3.3 mm diameter ceramic capillary for excitation currents of 190 ±5 kA with 10-90 % rise times of 11.5 ±1.5 ns.

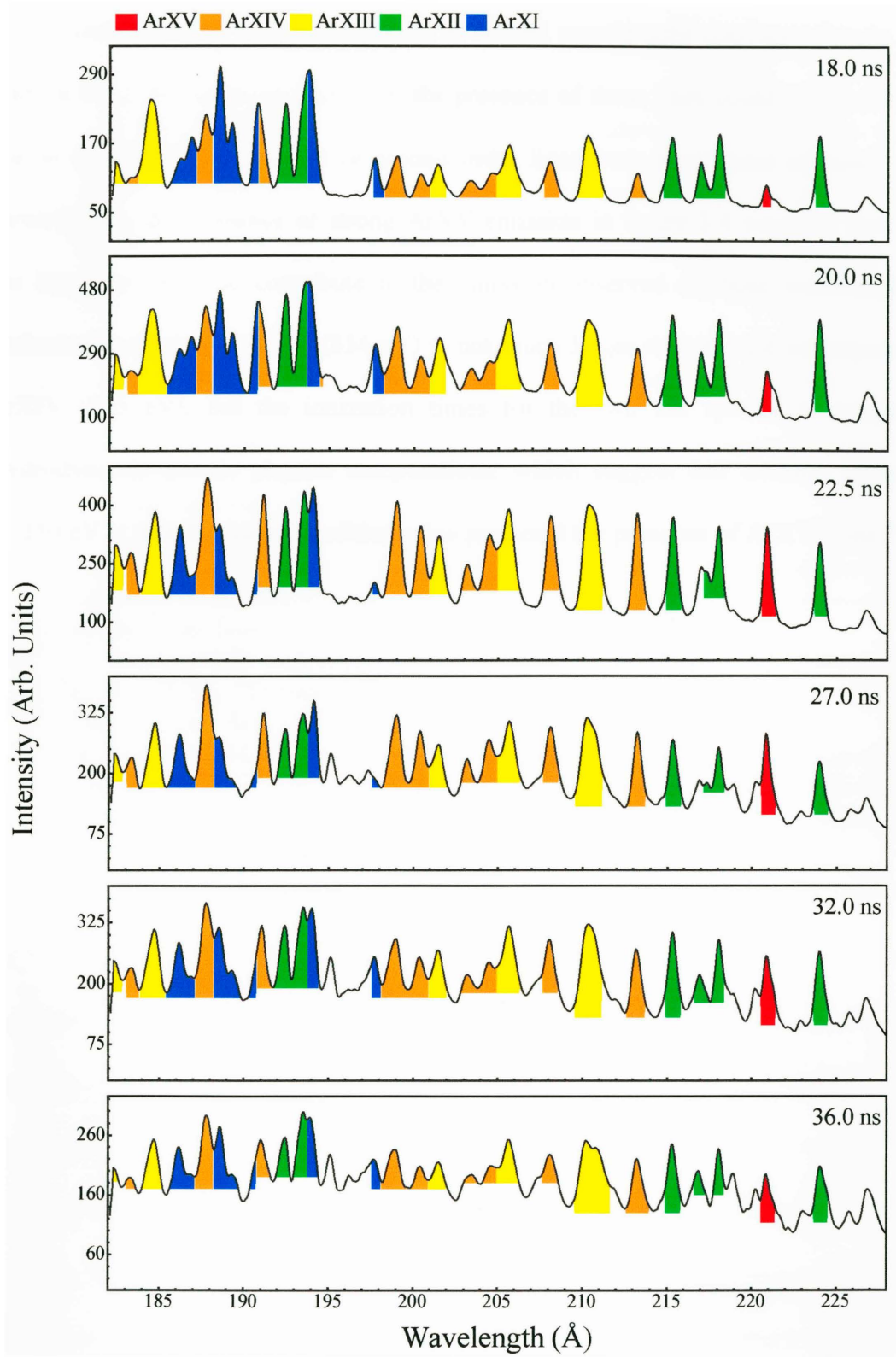

Figure 3.18. Time evolution of the degree of ionization in a 4 mm diameter ceramic capillary for excitation currents of 190 ±5 kA with 10-90 % rise times of 11.5 ±1.5 ns.

Line emission was also observed at several wavelengths corresponding to ArXVI lines in the 2-30 nm range. However, the presence of these lines could not be confirmed due to their overlap with first or second order lines from argon ions of lesser charge. Nevertheless, the presence of strong ArXV emission in figure 3.4 suggests that ArXVI ion lines are likely to contribute to the emission observed at those wavelengths (the ionization potential of ArXV (854 eV) is not much larger than are the corresponding to ArXIV (755 eV), but the ionization times for the two ion species is comparable). Hydrodynamic–atomic physics computations, which suggest and electron temperature $\geqslant$ 250 eV at this discharge conditions also predicted the presence of ArXVI ions [3.8].

3.4. References

3.1. V. N. Shlyaptsev, A. V. Gerusov, A. V. Vinogradov, J. J. Rocca, O. D. Cortazar, F. G. Tomasel and B. Szapiro, "Modeling of fast capillary discharge for collisionally excited soft x-ray lasers; comparison with experiments", *SPIE Proc. Ultra Short Wavelength Lasers II* **2012**, pp. 99-110, 1993.

3.2. J.J. Rocca, O. D. Cortazar, B. T. Szapiro, K. Floyd and F. G. Tomasel, "Fast-discharge excitation of hot capillary plasmas for soft-x-ray amplifiers", *Phys. Rev. E* **47**, pp. 1299-1304, 1993.

3.3. R. L. Kelly and L. J. Palumbo, 'Atomic and ionic Emission Lines Below 2000 Angstroms, Hydrogen Through Krypton", *NRL Report 7599*, Naval Research Laboratory, Washington 1973.

3.4. B.L. Henke, E.M. Gullikson and J.C. Davis, "X-ray interactions: photoabsorption, scattering, transmission, and reflection at E=50-30000 eV, Z=1-92", *Atomic Data and Nuclear Data Tables* **54**, pp. 181-342, 1993.

3.5. A. L. Osterheld, V. N. Shlyaptsev, J. Dunn, J. J. Rocca, M. C. Marconi, C. H. Moreno, J. J. Gonzalez, M. Frati, P. V. Nickles, M. P. Kalashnikov and W. Sandner, "Modeling of Laser produced Plasma and Z-Pinch X-Ray Lasers", *Proc. Of the X-ray Lasers Conf.*, pp. 353-362, 1998.

3.6. J.J. Rocca, V. N. Shlyaptsev, F. G. Tomasel, O. D. Cortazar, D. Hartshorn and J. L. A. Chilla, "Demonstration of a Discharge Pumped Table-Top Soft-X-Ray Laser", *Phys. Rev. Lett.* **73**, pp. 2192-2195, 1994.

3.7. A. L. Osterheld, V. N. Shlyaptsev, J. Dunn, J. J. Rocca, M. C. Marconi, C. H. Moreno, J. J. Gonzalez, M. Frati, P. V. Nickles, M. P. Kalashnikov and W. Sandner, "Modeling of Laser produced Plasma and Z-Pinch X-Ray Lasers", *Proc. Of the X-ray Lasers Conf.*, pp 353-362,1998.

3.8. V. N. Shlyaptsev, Private communication.

CHAPTER 4

SUMMARY

In conclusion, this thesis investigated the generation of capillary discharge plasma columns designed to reach significantly higher electron temperature and densities than those of previous experiments. The plasma columns were created by a new high power pulse generator designed and constructed as part of this work. The generator makes use of a three-stage compression scheme to generate the fast current pulses that excite the capillary plasmas. The final stage of the pulse generator consist in a water dielectric Blumlein transmission line capable of delivering current pulses up to 225 kA with 10-90 % rise times of ≅ 10 ns through the capillary load. Argon plasma columns were generated in polyacetal and alumina capillaries with diameters of 3 and 4 mm. The plasmas were characterized by means of time-resolved spectroscopy in the soft x-ray region and time-resolved pinhole images. The pinhole images show a rapid compression of the plasma column to a final diameter of ≅ 250 μm. The results showed that capillary plasmas with higher degrees of ionization are obtained when ceramic capillaries are utilized in comparison with polyacetal capillaries. Time-resolved spectra obtained in the 18-23 nm region at the time of maximum ionization are dominated by an ArXV line. The spectral data and model computations indicate an electron temperature > 250 eV has been

obtained, at discharge conditions at which model computations predict electron densities $> 1x10^{20}\,cm^{-3}$.

Future work continuing this research includes the direct measurement of the plasma electron density, e.g. utilizing line-broadening measurements of an added impurity. To realize the demonstration of lasing at shorter wavelengths, a way to inject metal vapors in the capillary load must be developed. Once reliable and uniform pre ionized columns are achieved, spectroscopic measurements in the soft x-ray spectral region must be carry out to evaluate the plasma conditions that are achieved. This must be followed by an optimization and search for the laser line.